# The Adsorption of Urea on Polycrystalline Gold Electrodes

A Thesis Submitted to the
College of Graduate Studies and Research
in Partial Fulfillment of the Requirements
for the degree of Master of Science
in the Department of Chemistry
University of Saskatchewan
Saskatoon

By
April Marie Woods

# Permission to Use

In presenting this thesis in partial fulfilment of the requirements for a Postgraduate degree from the University of Saskatchewan, I agree that the Libraries of this University may make it freely available for inspection. I further agree that permission for copying of this thesis in any manner, in whole or in part, for scholarly purposes may be granted by the professor or professors who supervised my thesis work or, in their absence, by the Head of the Department or the Dean of the College in which my thesis work was done. It is understood that any copying or publication or use of this thesis or parts thereof for financial gain shall not be allowed without my written permission. It is also understood that due recognition shall be given to me and to the University of Saskatchewan in any scholarly use which may be made of any material in my thesis.

Requests for permission to copy or to make other use of material in this thesis in whole or part should be addressed to:

Head of the Department of Chemistry

110 Science Place

University of Saskatchewan

Saskatoon, Saskatchewan

Canada

S7N 5C9

# Abstract

The adsorption of urea on Au polycrystalline electrodes was investigated using infrared spectroscopy, surface-enhanced infrared absorption (SEIRA) spectroscopy, electrochemistry, and spectroelectrochemistry. Electrochemical investigation indicates urea adsorption on a polycrystalline Au electrode at neutral pH as long as the surface is not oxidized. Partial urea desorption occurs at 0.5 V vs Ag/AgCl and above 0.8 V vs Ag/AgCl Au oxidation occurs, desorbing the remaining urea. Adsorption modes of urea were studied using SEIRA spectroscopy. Urea can adsorb in one of three configurations; through both nitrogen atoms (**I**), through a single nitrogen atom (**II**), or through the oxygen atom (**III**). In $H_2O$, adsorption occurs through both nitrogen atoms (**I**) and through a single nitrogen atom (**II**). For experiments in $D_2O$ adsorption occurs through both nitrogen atoms (**II**) and through the oxygen atom (**III**). The behavior of these adsorbates as a function of potential was studied using spectroelectrochemsitry, where an electrochemical cell with a Au coated IR window at the base is mounted on a benchtop spectrometer and the adsorbates at the surface are investigated as the applied potential is varied. In $H_2O$, at potentials of 0.9 V all of **II** has desorbed while some of **I** remains. In $D_2O$ experiments, at potentials of 0.9 V all of **III** has desorbed while some of **I** remains. Adsorption studies of various possible breakdown products of urea indicates that no known product is being formed.

# Acknowledgements

First of all I would like to thank my supervisor Dr. Ian Burgess for his support, patience and understanding. I would also like to thank Dr. Amanda Quirk for her endless wealth of knowledge and expertise.

I would also like to thank Ted Toporowski, Blair Chomyshen, and Jill Cornish in the Physics Machine Shop and our glassblower Rick Elvin for all of their excellent work and help in designing and creating the cell components that made this project possible, and Garth Wells at SyLMAND at the Canadian Light Source for the use of his sputtercoater.

Finally, I would like to thank my fiends and family for their curiousity, support and endless distractions and, most importantly, my husband for the love, support and encouragement.

To my husband, friends and family.

Thank you.

# Contents

# List of Tables

# List of Figures

# List of Abbreviations

| | |
|---|---|
| ATR | Attenuated Total Reflectance |
| CE | Counter Electrode |
| CV | Cyclic Voltammetry |
| DC | Differential Capacitance |
| DEMS | Differential Electrochemical Mass Spectrometry |
| EM | Electromagnetic |
| FTIRS | Fourier Transform Infrared Spectroscopy |
| IR | Infrared |
| IRRAS | Infrared Reflection-Absorption Spectroscopy |
| NMR | Nuclear Magnetic Resonance |
| OCP | Open Circuit Potential |
| RE | Reference Electrode |
| SEIRAS | Surface Enhanced Infrared Absorption Spectroscopy |
| SERS | Surface Enhanced Raman Spectroscopy |
| TDM | Transition Dipole Moment |
| UOR | Urea Oxidation Reaction |
| WE | Working Electrode |

# Chapter 1

# Introduction

Urea (Figure 1.1), one of the simplest amides, has a long and interesting history in the field of scientific research and holds major biological significance as it is a by-product of the metabolism of nitrogen containing compounds by animals. It is used in the body to excrete nitrogen, where two ammonia molecules and one carbon dioxide molecule are combined in the liver to form urea through the urea cycle.

Urea also plays a vital role in the nitrogen cycle. As a small molecule with two $NH_2$ groups that is excreted by most animals, it is abundant and a major source of nitrogen for plant life, so much so that bacteria have developed specific enzymes that can transform urea into a viable food source. Urease, the enzyme that hydrolyzes urea into ammonia and carbonate or ammonium carbamate (which is unstable and decomposes), is one of the most prolific and effective enzymes considering the simplicity of its target molecule.

Urea can potentially be found in interstellar ices [1]. Discussion of extraterrestrial considerations for urea includes its recycling on manned missions to space. All material needs

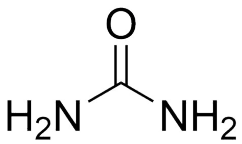


**Figure 1.1:** Molecular structure of urea.

to be recycled as much as possible therefore its capture and reuse, such as its degradation to useful molecules, is important.

## 1.1 Scientific significance of urea

Since its discovery by Rouelle in 1773 [2] urea has held a place of importance in the scientific community. Wöhler's synthesis of urea was a major scientific breakthrough that is still being studied today [3]. Urea was synthesized in a lab from inorganic compounds, Reaction 1.1, thus disproving the vitalist theory in which carbon-based compounds could only be made from living organisms [4].

$$\mathrm{Pb(OCN)_2 + 2NH_3 + H_2O \rightarrow PbO + NH_4OCN \rightarrow \underset{\text{(urea)}}{H_2NCONH_2}} \tag{1.1}$$

Research into the properties and uses of urea spans multiple fields of chemistry including coordination and quantum chemistry, biochemistry, spectroscopy and applied research.

Urea, as a small molecule, is curious because it has three potential coordination sites which makes it capable of forming complexes with different coordination numbers with several different metals [5]. Urea adsorbs to metal surfaces in different configurations depending on the nature of the metal surface [6–12]. Urea, even though it is a neutral molecule, exhibits reversible, structure sensitive anion like behavior upon urea adsorption on polycrystalline [12, 13] and single crystal platinum surfaces [6, 8, 14–16].

Multiple studies concerned with the structure and vibrational spectrum of urea have been performed using calculations of many descriptions. From the oldest calculations in the 1980s and 1990s to elucidate the structure of urea [17–24] to the determination of its vibrational

spectrum [20, 24–32] to the investigation of its adsorption configuration on metals [14, 33] it has been a popular molecule for quantum chemistry. To this day, more sophisticated calculations [3] are still being performed on old processes like Wöhler's synthesis of urea, first published in 1828 [4].

Aqueous urea solutions have properties that cause it to change the structures of proteins [34], increase the solubility of hydrophobic species [35] and prevent micelle formation [36], making it useful for the field of biochemistry.

In the field of spectroscopy; complexes, structures, and adsorption properties of urea are studied with techniques such as Nuclear Magnetic Resonance (NMR) [37], infrared [6–12], and Raman [38] spectroscopy and X-ray diffraction [39]. Infrared spectroscopy is a popular choices for investigating urea complexes and its adsorption configuration on metal surfaces.

Applications of urea include fertilizers and resins. Most soil bacteria have the enzyme urease which converts urea to carbon dioxide and ammonia, a necessary ingredient for plant life. Urea, in combination with formaldehyde, produce urea-formaldehyde resins. Extensive patent literature regarding urea attests to the importance of the small molecule in applied research and industry.

The electrochemical study of urea can be a first step in the study of related, more complex nitrogen containing molecules [6]. The adsorption behavior at electrode surfaces may also help elucidate the adsorption mechanisms and configurations of other related compounds.

## 1.2 Urea as an important industrial material

Urea is an incredibly important starting material and is used in many industrial applications with a production volume exceeding [40] 150 x $10^6$ t/yr in 2010. Ullmann's encyclopedia of Industrial Chemistry provides a general overview of industrially relevant reactions of urea [40]. With heating, urea decomposes primarily to ammonia and isocyanic acid (HNCO). In solution, urea isomerizes and is in equilibrium with two other structures [41, 42]. If the solution is dilute, the HNCO formed hydrolyzes to generate $NH_3$ and $CO_2$ [43]. With higher concentration solutions and relatively low temperature isocyanic acid (HNCO) reacts with urea to form biuret, triuret and cyanuric acid [44, 45]. Under the same conditions at higher temperatures, guanidine, ammelide, ammeline and melamine are also formed [45, 46]. Melamine can then be transformed into a resin using formaldehyde. Urea reacts with formaldehyde under acidic conditions to form methyleneurea, dimenthyleneurea and other methyleneureas which are used as slow release fertilizers. Reactions with formaldehyde under basic conditions form monomethylolurea and further reaction with formaldehyde yields dimethylolurea and other polymerization products. Urea reacts with $NO_x$ in the gas phase at high temperature and at lower temperature in solution to form $CO_2$, $N_2$ and $H_2O$, a reaction which is used to remove $NO_x$ from combustion gas [47].

## 1.3 Wastewater contamination and treatment

Urea production in humans depends heavily on protein intake [48] and the average healthy adult excretes around 30 grams of urea per day, most of it in urine [49]. In addition, the

production of urea from the reaction of ammonia and carbon dioxide at high temperature and pressure produces wastewater rich in urea. Purification occurs usually though hydrolysis [50] but other methods such as enzymatic urea hydrolysis [51, 52] and biological nitrification [53] are possible. The more complicated hydrolysis methods are generally costly and unsuitable for industrial scale or are still being tested. Electrolysis of wastewater producing hydrogen for use as a fuel source is an attractive prospect as it recycles animal excretion waste products that are produced with almost no effort [54, 55].

The urea oxidation reaction, denoted UOR occurs through Equation 1.2, and is part of the overall urea electrolysis reaction, Equation 1.3.

$$CO(NH_2)_2 + 6OH^- \rightarrow N_2 + CO_2 + 5H_2O + 6e^- \tag{1.2}$$

$$CO(NH_2)_2 + H_2O \rightarrow N_2 + 3H_2 + CO_2 \tag{1.3}$$

The UOR has slow kinetics due to a 6 $e^-$ transfer and complicated gas evolution steps [54] for $N_2$ and $CO_2$ [56–61] therefore rare and expensive noble-metal catalysts such as platinum/carbon [54] or rhodium [58] are required. Interest in producing catalysts made from cheaper and more abundant metals is growing and nickel is emerging as an attractive alternative [56, 59, 61–65].

## 1.4 Cyclic voltammetry

Cyclic voltammetry provides information on processes occurring at the electrode surface involving the transfer of electrons such as oxidation/reduction and adsorption/desorption. The resulting voltammogram provides information about the potential regions where processes are occurring that can then be probed by a complementary technique like infrared (IR) spectroscopy which provides structural information. The charge passed during certain processes can also provide information on the charge of adsorbing species and surface coverage.

Information on the oxidation of urea can be obtained from cyclic voltammetry. The shape of the resulting voltammogram provides information on the type of reaction occurring. In the case of urea, oxidation on metals like platinum and rhodium exhibit normal behavior, while the oxidation of urea on nickel at high pH exhibits catalytic behavior. Electrode poisoning occurs at more positive potentials which halts the catalytic behavior. This complicated overall electrochemical process is interesting and merits further study because its mechanism is not understood.

## 1.5 Surface-Enhanced Infrared Absorption Spectroscopy (SEIRAS)

To investigate the adsorption of urea on a metal surface requires a technique which is sensitive to adsorbed molecules compared to those in solution and which can measure signal from a very low concentration of adsorbed molecules. SEIRAS achieves this by taking advantage of IR measurements in the attenuated total reflectance (ATR) configuration, which inherently

samples solution near the IR element surface, and the phenomenon of surface enhancement, discussed in section 3.5. Other IR spectroscopy techniques have been used to study the adsorption of urea onto metals such as platinum [6–8, 10, 12] and rhodium [6–9]. A single investigation of the adsorption of urea on gold has been performed [11]. More recently, SEIRAS has been used to study the adsorption of 4-methoxypyridine on gold films [66] and ubiquinone in hybrid bilayer membranes supported on gold films [67].

## 1.6 Thesis objectives

The adsorption configuration of urea has been studied extensively on platinum and ruthenium with limited characterization on gold. No studies using SEIRAS have been performed on urea. This technique has an advantage in that the behavior at the surface can be investigated without interference from solution phase species. As gold is one of the metals that gives rise to the strongest surface enhancement effect, it will be used to study the adsorption behavior of urea using SEIRAS, building on previous work done in the group.

The long term goal of this project is to develop a method to investigate electrochemical processes occurring at the electrode surface on metals other than gold. The method developed would ideally be able to be performed using a benchtop spectrometer with a traditional globar source that does not require the use of a high brilliance light source like a synchrotron to achieve adequate signal. SEIRAS has already been proven using gold surfaces, and now the focus is to implement it in investigation of other metal surfaces. Gold is expensive, and the study of interesting electrochemical processes on other metals can elucidate which of these metals would result in appropriate catalysts for processes such as wastewater treat-

ment. Ultimately, urea was chosen as a probe molecule due to its interesting electrochemical processes on nickel electrodes and extensive literature presence.

In the short term, this project aims to investigate urea adsorption on gold to provide a well characterized reference for the eventual experiments on nickel and filling a gap in the literature regarding SEIRAS investigations of urea adsorption on gold in neutral media.

# Chapter 2

# Literature Review

## 2.1 The structure of urea

Early work in the determination of the structure of urea was performed using primarily chemical analyses. The focus was to determine whether urea existed in the classical structure (Figure 2.1**A**), an isomeric one (Figure 2.1**B**) or in the zwitterion-type structure (Figure 2.1**C**, adapted from Reference [68]) [68]. At this time, urea was thought to exist in a non-planar conformation. The reaction between urea and nitrous acid pointed towards a zwitterionic structure, Figure 2.1**C**, and suggested that a tautomeric equilibrium existed between **A** and **C** [69]. Studies of the dipole moments of urea and its derivatives indicated that the zwitterion exists to a large extent in solution but no value could be deduced [70–72]. In 1937, Pauling *et al.* investigated the dependence of interatomic distances on single bond-double bond resonance and determine a 28 % double bond character for the C-N bond in urea, which suggested a planar structure [73].

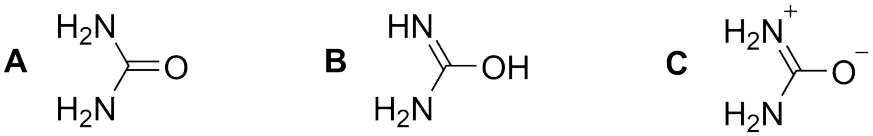


**Figure 2.1:** Potential structures of urea. Adapted from reference [68]

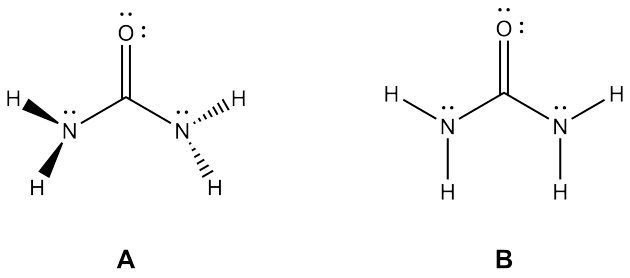


**Figure 2.2:** Two structures of urea with potential hydrogen positions. A) Hydrogens in a plane perpendicular to the rest of the atoms and B) in a plane with the rest of the atoms.

Early X-ray experiments on solid urea investigated the scattering power of light atoms such as carbon, oxygen and nitrogen and determined the atoms existed in a single plane but due to the lightness of the hydrogen atoms the exact positions had to be inferred [74–80]. Figure 2.2 shows the two possible configurations of the hydrogen atoms in the urea molecule. Figure 2.2**A** shows urea with the hydrogen atoms in a plane perpendicular to the rest of the atoms and Figure 2.2**B** shows the hydrogen atoms in a plane parallel with the rest of the atoms.

In the late 1950s neutron scattering experiments confirmed the results that X-ray experiments were unable to prove: that the hydrogen atoms, in the solid state, were in the same plane as the rest of the atoms (Figure 2.2**B**) [80–83].

Studies were also performed to determine the geometry of urea in the gas phase. Early geometry optimization and frequency calculations predicted that urea in the gas phase existed as it did in the solid phase: with the hydrogen atoms lying in the same plane as the oxygen, nitrogen and carbon atoms (Figure 2.2**B**) [17–20]. Experimental data, however, indicated that gas phase urea must exist in a non-planar structure [84–87]. Calculations by numerous groups in 1992–1993 showed it to be non-planar in the gas phase [20–24]. Ab initio calculation

of gases with better models and computing power indicated that urea exists as a non-planar molecule in the gas phase [88].

Monte Carlo simulations of liquids from the same study were inconclusive in determining the configuration of urea in water, but indicated that the solvent does not impose a significant energy barrier to rotation about the nitrogen atom. Calculations for isolated urea indicated that it interconverts between $C_s$ and $C_{2v}$ symmetries through $NH_2$ torsion and $NH_2$ inversion motions [89]. The planarity of solid urea is due to the extensive hydrogen bonding present in the solid. In solution, the urea-urea hydrogen bonds which gives solid urea its planar structure are not present. Instead, hydrogen bonding is present from water which gives urea a structure that is intermediate between a structure of the gas and solid phase [26].

## 2.2 Vibrational analysis of urea in the solid, gas and aqueous phase

In 1941, Kellner performed a vibrational analysis of urea assuming a model where the hydrogen atoms were in a plane perpendicular to the remaining atoms [25]. The assignments were made by comparing calculated values to those determined experimentally using Raman spectroscopy, summarized in Table 2.1. The force constants of a bond are approximately proportional to the strength of the bond, which indicated that the CN bonds had some double bond character and the CO bond had approximately the same amount of single bond character [90]. Force constants were determine for the CO and CN bonds to be 9.7 x $10^5$ and 4.86 x $10^5$ dynes/cm respectively. Comparing the force constant for CO to the value determined for formaldehyde by Sutherland and Dennison (13.45x$10^5$ dynes/cm) indicated

| Vibrational frequency ($cm^{-1}$) | Assignment |
|---|---|
| 1008 | $\nu$CN |
| 1167 | deformation vibration |
| 1604 | deformation vibration |
| 1680 | $\nu$CO |
| 3385 | $\nu_s$NH |

**Table 2.1:** Summary of vibrational assignments from reference [25]

a weakening of the force constant [91] by 39 %. Similarly, comparing the force constant of the CN bond to those for a CN single bond in methylamine, 4.86 x $10^5$ dynes/cm, and a CN triple bond in cyanide, 17.9 x $10^5$ dynes/cm, indicates it is much closer to the value for a single bond [92], with a strengthening of 35 %.

The development of more sophisticated analysis aimed to dispel contradictions and uncertainties arising from former interpretations. Vibrational analysis of urea in the solid phase were measured for various $^2$H, $^{13}$C, $^{15}N_2$, and $^{18}$O analogues [26]. Raman spectra were measured of urea-water solution as well as force field calculations of gas phase and solid state urea.

Keuleers *et al.* attribute the "misunderstandings" in the literature to structural effects between urea in the gas and solid phases. Urea in the aqueous phase exists in a structure intermediate between the structures of the gas and solid phase. As a solid, the nitrogen atoms are in a trigonal planar conformation, Figure 2.2B, leading to increased conjugation between the nitrogen and CO bond and a greater contribution from its resonance forms (Figure 2.1C) compared to urea in the gas phase which has $sp^3$ hybridization (Figure 2.2A). Consequently, there is less double bond character in the CO bond and more double bond character in the CN bonds in solid urea compared to the gas phase leading to a shift to lower CO and

| ($cm^{-1}$) | $CO(NH_2)_{2(s)}$ | $CO(NH_2)_{2(aq)}$ | $CO(NH_2)_{2(g)}$ |
|---|---|---|---|
| $\nu$(CO) | 1540 | 1664 | 1731 |
| $NH_2$ deform. | 1647 | 1626 | 1600 |
| $NH_2$ deform. | 1623 | 1593 | 1589 |
| $\nu_{as}$(CN) | 1466 | 1461 | 1386 |
| $\nu_s$(CN) | 1010 | 1003 | 934 |

**Table 2.2:** Vibrational frequencies of urea in the solid, gas and aqueous phases

higher CN frequencies. Hydrogen bonding in solid urea between the hydrogen and oxygen atoms in urea cause a shortening of the CN bonds and a lengthening of the CO and NH bonds, leading to shift to higher frequencies in the case of CN bonds (both symmetric and asymmetric stretching vibrations) and a lower frequency in the case of the NH, $NH_2$, and CO bonds. As urea gas phase experiments could not be performed, experiments on urea-water solutions were used as a substitute [26]. Table 2.2 shows that vibrational frequencies for urea in the gas, aqueous and solid phase cannot be directly compared.

Keuleers *et al.* studied urea in the solid and aqueous phases [26]. In solid urea two peaks and two shoulders appeared at 3444, 3349, 3450 (sh) and 3341 (sh) $cm^{-1}$. These were assigned to $\nu_{as}(NH_2)$, $\nu_s(NH_2)$, $\nu_{as}(NH_2)$, and $\nu_s(NH_2)$, respectively. These assignments, and additional urea vibrational frequencies are summarized in Table 2.3.

Four absorptions are expected in the 1700-1400 $cm^{-1}$ region for sold urea: the $\nu$(CO), $\nu_{as}$(CN), $\delta_{as}(NH_2)$ and $\delta_s(NH_2)$. Two of these, the $\nu_{as}$(CN) and $\delta_{as}(NH_2)$, appear at 1625 and 1466 $cm^{-1}$, respectively and agree with literature [20, 24, 27–32, 93–99]. The relative positions of the two remaining absorptions, $\delta_{as}(NH_2)$ and $\nu$(CO), is an area of disagreement in the literature. The assignment of the higher frequency peak as $\nu$(CO) has been supported by normal coordinate analysis (with coupling effects) [27], Hartree-Fock [28] and MP2 cal-

| | urea ($cm^{-1}$) | urea $^{13}C$ ($cm^{-1}$) | urea $^{15}N_2$ ($cm^{-1}$) | urea $^{18}O$ ($cm^{-1}$) | urea-$d_4$ ($cm^{-1}$) |
|---|---|---|---|---|---|
| $\nu_{as}(NH_2)$ | 3450 | 3454 | 3443 | 3450 | 2601 |
| $\nu_{as}(NH_2)$ | 3444 | 3443 | 3435 | 3445 | 2593 |
| $\nu_s(NH_2)$ | 3349 | 3344 | 3341 | 3347 | 2440 |
| $\nu_s(NH_2)$ | 3341 | 3340 | 3320 | 3330 | 2433 |
| $\delta_s(NH_2)$ | 1683 | 1673 | 1676 | 1675 | – |
| $\delta_{as}(NH_2)$ | 1625 | 1622 | 1613 | 1625 | – |
| $\nu(CO)$ | 1601 | 1573 | 1600 | 1592 | 1608 |
| $\nu_{as}(CN)$ | 1466 | 1434 | 1460 | 1465 | 1480 |

**Table 2.3:** Vibrational assignments of urea from infrared spectroscopy of solid urea from Keuleers *et al.*, reference [26]

culations [24], and by comparing characteristic frequency values to the infrared structural correlation chart [20]. The coupling between these vibrations, $\delta_{as}(NH_2)$ and $\nu(CO)$, has already been stated [95, 98]. The opposite assignment where the lower frequency peak is $\nu(CO)$ has been supported by normal coordinate analyses [29–32], measurements of the Raman and infrared spectra of the $^{18}O$ and $^{15}N$ isotopomers [95, 98], and finally using intermolecular energy functions to reproduce Raman and infrared spectra [97]. Keuleers *et al.* confirmed that absorbances at 1683 and 1625 $cm^{-1}$ were due to $NH_2$ vibrations as both of these peaks disappeared upon deuteration. Shifts in the other two absorbances, 1601 to 1608 $cm^{-1}$ and 1466 to c.a. 1480 $cm^{-1}$ indicate strong coupling between these and the NH bonds.

Assignment for the urea-water solution can be done by comparing peak positions obtained by Raman spectroscopy to those obtained for solid urea by IR and is summarized in Table 2.4. All four absorbances present in IR spectroscopy are also present in Raman with the addition of two more peaks at 1648 and 1540 $cm^{-1}$. These are attributed to crystal field

| IR | Raman | |
|---|---|---|
| Wavenumber ($cm^{-1}$) | Wavenumber ($cm^{-1}$) | Assignment |
| 1683 | 1647 | $\delta_s(NH_2)$ |
| – | 1648 | $\nu(CO)$ + $\delta_s(NH_2$ character) |
| 1625 | 1623 | $\delta_{as}(NH_2)$ |
| 1601 | 1540 | $\nu(CO)$ |
| – | 1540 | $\nu(CO)$ character mainly |
| 1466 | 1466 | $\nu_{as}(CN)$ |

**Table 2.4:** Assignment of absorbances in the 1700–1400 $cm^{-1}$ region of the Raman spectrum of a urea-water solution

splitting and has already been observed for Raman studies of single crystal urea [100, 101]. Vibrations that result in a change in dipole moment of a bond are IR active and vibrations that result in a change in polarizability are Raman active and are not mutually exclusive for non-centrosymmetric molecules.

## 2.3 Urea adsorption on metal surfaces

With advancements in surface sensitive techniques the adsorption of urea on metal surfaces became widely studied for potential applications in catalysis, a starting point for the study of larger, more complicated nitrogen containing compounds, and as a useful probe for metal surface characterization. The adsorption of urea on platinum in acidic media is well studied and can be used to elucidate the adsorption modes of urea on analogous metals like rhodium.

Figure 2.3 shows the possible bonding modes of urea adsorbed on a metal. The four possible bonding modes of urea are 2N-bonded, N-bonded, O-bonded with the $\nu(CO)$ axis tilted and O-bonded with the $\nu(CO)$ axis parallel to the surface and will be referred to as

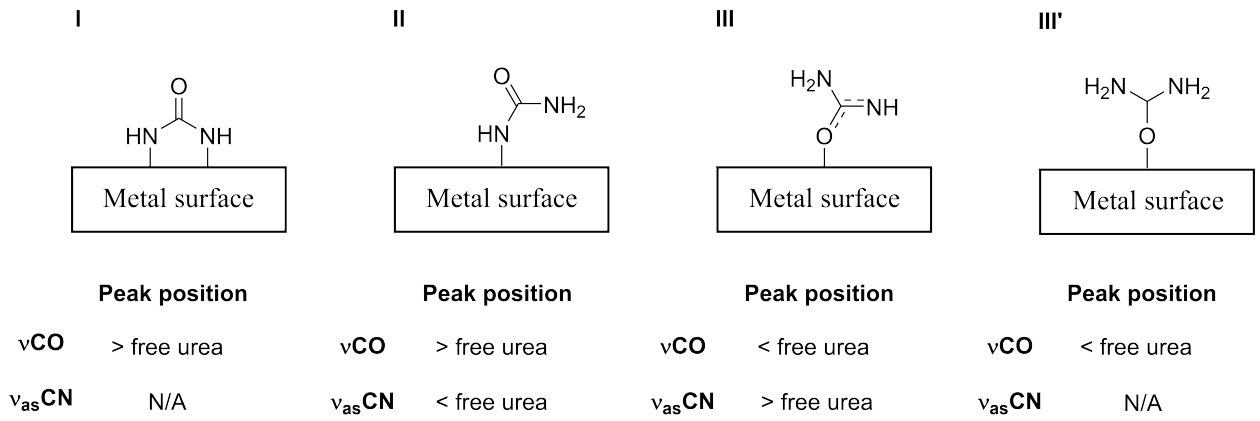


**Figure 2.3:** Different bonding modes of urea to metal surfaces. From left to right: **mode I**) 2N-bonded; **mode II**) N-bonded; **mode III**) O-bonded (tilting); **mode III′)** O-bonded (normal). Table indicates the shift in $\nu$(CO) and $\nu_{as}$(CN) peak position for each bonding mode compared to free urea.

**mode I**, **mode II**, **mode III** and **mode III′**, respectively, for the remainder of this thesis. Bidentate adsorption through the oxygen and nitrogen atoms is not known to occur.

The majority of urea-metal adsorption studies have been performed on platinum surfaces. Wieckowski and Rikvold produced theoretical models of the adsorption of urea on Pt(100) [14]. The assumption that urea adsorbed through both nitrogen atoms with the transfer of two electrons per adsorbed molecule produced models that agreed with voltammetric results [15, 102–104].

Bezerra *et al.* studied the behavior of urea on polycrystalline platinum during the initial steps of electrochemical oxidation using *in situ* Fourier transform infrared spectroscopy (FTIRS) at acidic, neutral and basic pH using s-and p-polarized light to distinguish between peaks occurring from solution and adsorbed urea species, respectively [12]. Experiments were performed at a relatively high urea concentration (0.1 M) with 0.1 M supporting electrolyte ($DClO_4$, KF or KOD) in $D_2O$. Using s-polarized light perdeuterated urea in acidic solution shows two upward peaks at 1608 and 1467 $cm^{-1}$ which correspond to the $\nu$(CO) and

$\nu_{as}$(CN) vibrational frequencies of deuterated free urea, respectively. The upward direction of the peaks indicate a the loss of urea in the thin layer cavity through acid mediated hydrolysis in solution and oxidation at high potentials (0.45 V vs Ag/AgCl). With p-polarized light, two new downward peaks appear in the spectra for the same system at 2030 and 1792 $cm^{-1}$ and are attributed to adsorbed carbon monoxide produced from the decomposition of urea in the a-top and multicoordinated forms. Upward peaks from the loss of urea are also observed at 1604 and 1493 $cm^{-1}$ using p-polarized light. A shoulder appears at 1617-1629 $cm^{-1}$, and is attributed to $\nu$(CO) of urea. These results led to the conclusion that urea adsorbed through two nitrogen atoms in the potential range studied (0.15 -0.35 V vs Ag/AgCl). Differential electrochemical mass spectrometry (DEMS) experiments indicated $N_2$ as an oxidation product which, due to its structure, cannot be observed with IR spectroscopy [13]. In neutral solution, peaks at 2161, 1631, 1608, 1418, and 1364 $cm^{-1}$ are observed. Only the peak at 2161 $cm^{-1}$ is not observed with both s-and p-polarized light[12]. Tentative assignments are as follows: 2161 $cm^{-1}$ from cyanate ion, 1631 $cm^{-1}$ from dissolved $NO_2$, 1608 $cm^{-1}$ from $\nu$(CO) of dissolved urea, 1418 $cm^{-1}$ from trans $[N_2O_2]^{2-}$ and 1364 $cm^{-1}$ due to $NO_3^-$. Assignment of nitrogen containing products was done based on band position and previous studies using DEMS which indicated $NO_2$ and $N_2O$ as volatile products of urea oxidation [13].

In alkaline solution [12], two peaks are observed using s-polarized light at 1608 and 1499 $cm^{-1}$, the $\nu$(CO) and $\nu_{as}$(CN) of free urea in solution, respectively. With p-polarized light and no applied potential three peaks are observed at 2020, 1556, and 1465 $cm^{-1}$ for adsorbed urea. These peaks are attributed to adsorbed carbon monoxide, $\nu$(CO) and $\nu_{as}$(CN) of adsorbed urea, respectively. At more negative potentials, less than -0.4 V, the $\nu_{as}$(CN) is strongest while at potentials greater than -0.4 V, its intensity decreases and the peak for

$\nu$(CO) increases indicating that urea is adsorbed through a single nitrogen atom at low potentials, **mode II**, and through the oxygen atom at high potentials, **mode III**, based on the relative intensities of the peaks. A weak peak attributed to carbon monoxide at 2020 $cm^{-1}$ is observed at all potentials. No solution species were reported.

Climent *et al.* studied the adsorption of urea on Pt(100), Ru(100), and Pt(111) using electrochemical Fourier-Transform Infrared Spectroscopy (FTIRS) [6]. Experiments were performed using s and p-polarized light with a low urea concentration (1 mM urea) in 0.1 M $HClO_4$ in $D_2O$. In acidic solution on Pt(100) urea adsorbs spontaneously as an adlayer and is stable to rinsing. The loss of peaks with applied potential at 1500 ($\nu_{as}$(CN)) and 1600 $cm^{-1}$ ($\nu$(CO)) arising from urea, in both s and p-polarized experiments indicate the loss of solution phase and adsorbed urea, and the formation of a single peak at 1701 $cm^{-1}$ collected with p-polarized light indicates urea adsorption. As there is only one peak present at 1701 $cm^{-1}$ and it is above the frequency of the $\nu$(CO) peak of free urea, 1610 $cm^{-1}$, Climent *et al.* concluded that urea adsorbs through the nitrogen atom [29]. The absence of a $\nu_{as}$(CN) peak indicates the urea must be normal to the surface, resulting in a dynamic dipole parallel to the surface and adsorbed though both nitrogen atoms, **mode I**. The shift in $\nu$(CO) peak position as a function of potential is due to lateral interactions at more negative potentials (and low coverage) and due to a shift in peak position as a function of external electric field, at high potentials and high coverage [6].

Urea adsorption on Pt(100) and Rh(100) at oxidative potentials was investigated by stepping to increasingly more positive potentials [7]. A low urea concentration (1 mM urea) in 0.1 M $HClO_4$ in $D_2O$ was used. The urea adlayers formed on both platinum and rhodium were strongly adsorbed and showed the same trend: upon increasing the potential to 0.34

V vs Ag/AgCl the $\nu$(CO) (1602 $cm^{-1}$) and $\nu_{as}$(CN) (1497 $cm^{-1}$) peaks from solution phase urea were lost and a higher frequency peak at 1682 $cm^{-1}$ was formed. From information on the surface coverage, determined from radiotracer [102] and Auger electron spectroscopy [16], and the peak positions and behavior Climent *et al.* determined that urea adsorbed through a two electron process and, as no new peak appeared for $\nu_{as}$(CN), must be adsorbed parallel to the surface through both nitrogen atoms, **mode I**.

Climent *et al.* extended their investigation to Pt(111) surfaces [8] with 0.1 mM urea and 0.1 M $HClO_4$ in $D_2O$. On Pt(111), unlike Pt(100), urea has two distinct bonding modes. At potentials below 0.24 V vs Ag/AgCl, urea is bonded through a single nitrogen atom, **mode II**, and at potentials above 0.24 V vs Ag/AgCl it is bonded through the oxygen atom, **mode III**. These assignments were determined from the frequency shifts from 1625 $cm^{-1}$ to 1522 $cm^{-1}$ for $\nu$(CO) and 1445 $cm^{-1}$ to 1348 $cm^{-1}$ for $\nu_{as}$(CN). In both modes the molecule is tilted with respect to the surface determined from the presence of a peak from the $\nu_{as}$(CN) at low potentials and a higher than expected $\nu_{as}$(CN) peak at high potentials. From voltammetry experiments it was determined that adsorption occurs through a one electron process regardless of the applied potential. Urea does not adsorb as strongly on Pt(111) as on Pt(100). On Pt(111) urea is competing with oxygenated species for adsorption sites at high positive potentials.

Climent *et al.* studied the adsorption of 1 mM urea in 0.1 M $HClO_4$ in $D_2O$ on Pt(110) surfaces using electrochemical techniques and FTIRS with s and p-polarized light [10]. From charge displacement experiments they were able to determine that urea adsorbs through a one electron process. Two peaks were observed using s-polarized light at 1609 $cm^{-1}$ and 1500 $cm^{-1}$ from the $\nu$(CO) and $\nu_{as}$(CN) stretches of solution phase urea, respectively. As with

Pt(111), urea on Pt(110) has two different bonding modes. Below 0.34 V vs Ag/AgCl the $\nu$(CO) peak for adsorbed urea appears at 1627 $cm^{-1}$ and shifts to 1580 $cm^{-1}$ above 0.34 V vs Ag/AgCl. Initially, urea is adsorbed through a single nitrogen atom but changes orientation to adsorb through the oxygen atom at high potentials. The $\nu_{as}$(CN) peak of adsorbed urea overlaps with those of solution peaks (upward going urea peaks) and a clear analysis could not be performed. The presence of the peak at 1500 $cm^{-1}$ indicates that urea is most likely tilted with respect to the electrode surface [10].

Finally, Climent *et al.* studied the adsorption of urea on different rhodium crystal faces using electrochemical techniques and FTIRS [9]. Rhodium was chosen as it is a homologous surface to Pt(100). Experiments were performed using 1 mM urea in 0.1 M $HClO_4$ in $D_2O$. It was found that on Rh(100) urea adsorbed irreversibly and is bonded through both nitrogen atoms with a single peak at 1612–1638 cm $^{-1}$, **mode I**, regardless of potential or coverage. On Rh(110) it was found that urea adsorbed through the oxygen atom at potentials below 0.44 V vs Ag/AgCl with $\nu$(CO) and $\nu_{as}$(CN) at 1548–1563 $cm^{-1}$ and 1380 $cm^{-1}$ (**mode III**) and above 0.44 V vs Ag/AgCl through a single nitrogen atom with $\nu$(CO) and $\nu_{as}$(CN) at 1636-1651 $cm^{-1}$ and 1338 $cm^{-1}$ (**mode I**) and was adsorbed competitively with oxygenated species. On Rh(111) it was found that urea was adsorbed through the oxygen atom regardless of potential and tilted slightly at high potentials where the coverage was at a maximum. Below 0.34 V vs Ag/AgCl peaks for $\nu$(CO) and $\nu_{as}$(CN) were at 1575 and 1397 $cm^{-1}$, and above 0.34 V vs Ag/AgCl the $\nu$(CO) disappears due to the high degree of tilting and $\nu_{as}$(CN) appears at 1369 $cm^{-1}$. These findings are very similar to platinum in all respects.

The adsorption configuration of urea on Pt(100) was investigated using density functional calculations [33]. Comparing urea adsorption to that of the ureylene biradical formed via

the loss of two hydrogen atoms and transfer of two electrons shows that the biradical species gave vibrational frequencies that best match experimental results presented by Climent *et al.* [6].

Adsorption of urea on polycrystalline gold was studied using cyclic voltammetry, tensammetry and SERS using 0.01 M urea in 0.1 M $HClO_4$ or 0.1 M $KClO_4$ in $H_2O$. In neutral solution, it was determined that urea adsorbs through the oxygen atom to the gold surface. Adsorption experiments were attempted in acidic solution but no SERS peaks attributed to adsorbed urea were observed, only adsorbed hydrolysis products of urea [38]: $CO_2$ and $NH_4^+$.

*In situ* FTIRS and cyclic voltammetry were used to investigate the adsorption of 0.005 M $D_4$-urea on Au(100) and Au(111) electrodes in 0.1 M HF in $D_2O$ [11]. By comparing the measured charge density of urea adsorption to Au(100) to that of urea adsorption to platinum indicated adsorption to Au(100) occurred without dissociation of the NH bonds. For urea adsorption on Au(100) at low potentials (-0.017–0.163 V vs Ag/AgCl) a single peak appears at 1555 $cm^{-1}$ and decreases in intensity with increasing potential and disappears at 0.703 V vs Ag/AgCl. A second peak appears at 1628 $cm^{-1}$ at more positive potentials, 0.433 V vs Ag/AgCl, and increases in intensity as the 1555 cm $^{-1}$ peak decreases. Both peaks are due to the $\nu$(CO) of urea adsorbed in different modes. The absence of a $\nu_{as}$(CN) indicates that the $\nu$(CO) bond is normal to the surface but the peak position does not indicate whether urea is adsorbed through the oxygen or nitrogen atoms due to its similarity with that of free urea at 1610 $cm^{-1}$. For urea adsorption on Au(111) two peaks are observed at all potentials: 1560 and 1380 $cm^{-1}$. The peaks arise from the $\nu$(CO) and $\nu_{as}$(CN) vibrational frequencies of adsorbed urea. Due to the shift of the $\nu_{as}$(CN) peak to lower wavenumbers urea must be adsorbing through a single nitrogen atom, **mode II**. The $\nu$(CO) peak, which does not shift

upon carrying out the same experiment in $H_2O$ with $H_4$-urea, must be from O-bonded urea, **mode III**, therefore two adsorbates are found on Au(111).

Table 2.5 summarizes literature results of urea adsorption on different metals, crystal faces and applied potentials.

Some spectroscopic characterization of the adsorption of urea on gold surfaces has been performed using SERS and *in situ* FTIRS but limited information is provided. In addition, the majority of adsorption studies are performed in acidic media, with limited interest given to processes occurring in neutral or basic media. Finally, no SEIRAS studies have been performed on the adsorption of urea. The use of gold in SEIRAS experiments is emerging as a powerful experimental method for the investigation of the adsorption configuration of molecules [66] and the study of more complicated, biologically relevant systems [67] in this group.

| Metal | Face | Electrochemistry | Orientation | Peaks ($cm^{-1}$ ) |
|---|---|---|---|---|
| Pt | (100) | Irreversibly adsorbed | **mode I**, all E | **S-polarized light:** 1609 ↑ 1500 ↑<br>**P-polarized light:** 1701 ↓ 1609 ↑ 1500 ↑ |
| | (110) | Reversibly adsorbed | Low E: **mode II** (unclear, likely tilted)<br>High E: **mode III** (unclear, likely tilted) | **S-polarized light:** 1605 ↑ 1498 ↑<br>**P-polarized light:** 0.3–0.5 V: 1622 ↓; 0.5–0.80 V: 1627 ↓ 1510 ↓ |
| | (111) | Reversibly adsorbed | Low E: **mode II**<br>High E: **mode III** | **S-polarized light:** 1609 ↑ 1500 ↑<br>**P-polarized light:** 0.45 V: 1623 ↓ 1444 ↓; 0.70 V: 1523 ↓ 1342 ↓ |
| Rh | (100) | Irreversibly adsorbed | **mode I**, all E | **S-polarized light:** 1600 ↑ 1497 ↑<br>**P-polarized light:** 1612–1638 ↓ |
| | (110) | Competitive adsorption at high E with oxygenated species | Low E: **mode III**<br>High E: **mode II** | **S-polarized light:** 1605 ↑, 1497 ↑<br>**P-polarized light:** 0.3V–0.4V: 1548–1563 ↓ 1380 ↓; 0.4–0.7 V: 1636–1651 ↓ 1338 ↓ |
| | (111) | Mixed behavior | Low E: **mode III**<br>High E: **mode III** (more tilted) | **S-polarized light:** 1605 ↑ 1494 ↑<br>**P-polarized light:** 0.20–0.60V: 1575 ↓ 1397 ↓; 0.60–0.90 V: 1369 ↓ |
| Au | (100) | Competitive adsorption with electrolyte anions | $\nu$(CO) axis perpendicular | 0.18–0.88 V: 1550–1576 ↓; 0.73–1.08 V: 1601–1625 ↓ |
| | (111) | Competitive adsorption with electrolyte molecules | **mode II** and **mode III** | 1.28–0.98 V: 1577–1545 ↓; 1.28–0.88 V: 1380 ↓ |

**Table 2.5:** Adsorption behavior of urea at various metals and faces taken from the literature. ↑ indicates upward going peak, ↓ indicates downward going peak.

## 2.4 Reactions involving urea

Urea has many pathways and possible reactions, mostly involving hydrolysis, summarized in Scheme 2.1. It is important to discuss these reactions as various products may be generated and contribute to SEIRAS signals.

### 2.4.1 Hydrolysis

Hydrolysis of urea in solution occurs with and without the presence of urease, an enzyme which catalyzes the hydrolysis of urea. The products formed depend on the reaction conditions but, in general, reaction in the presence of urease favors hydrolysis products while the absence of urease favors the elimination of ammonia, Scheme 2.1 structure **1** [105]. The rate enhancement of urease [106] compared to urea hydrolysis in the absence of the enzyme ($k_{cat}/k_{uncat}$) was calculated to be 3 x $10^{15}$. Without urease, elimination of ammonia is favored and is initiated by a proton transfer between the two amino groups mediated by a single water molecule [105]. The relative rate of elimination over hydrolysis without urease in neutral media was calculated to be ∼150 which agrees with recent experimental estimates [106].

In the presence of urease, urea will hydrolyze spontaneously to give $HCO_3^-$ and $NH_4^+$ in phosphate (pH = 7.5 and 6.7) and maleate (pH = 6.7) buffers, Scheme 2.1 structure **2**, while it hydrolyzes in the presence of citrate (pH = 6.7) and Tris (pH = 7.5) buffers to give ammonium carbamate, Scheme 2.1 structure **3** [107]. These differences were attributed to buffer effects and ammonium ion inhibition.

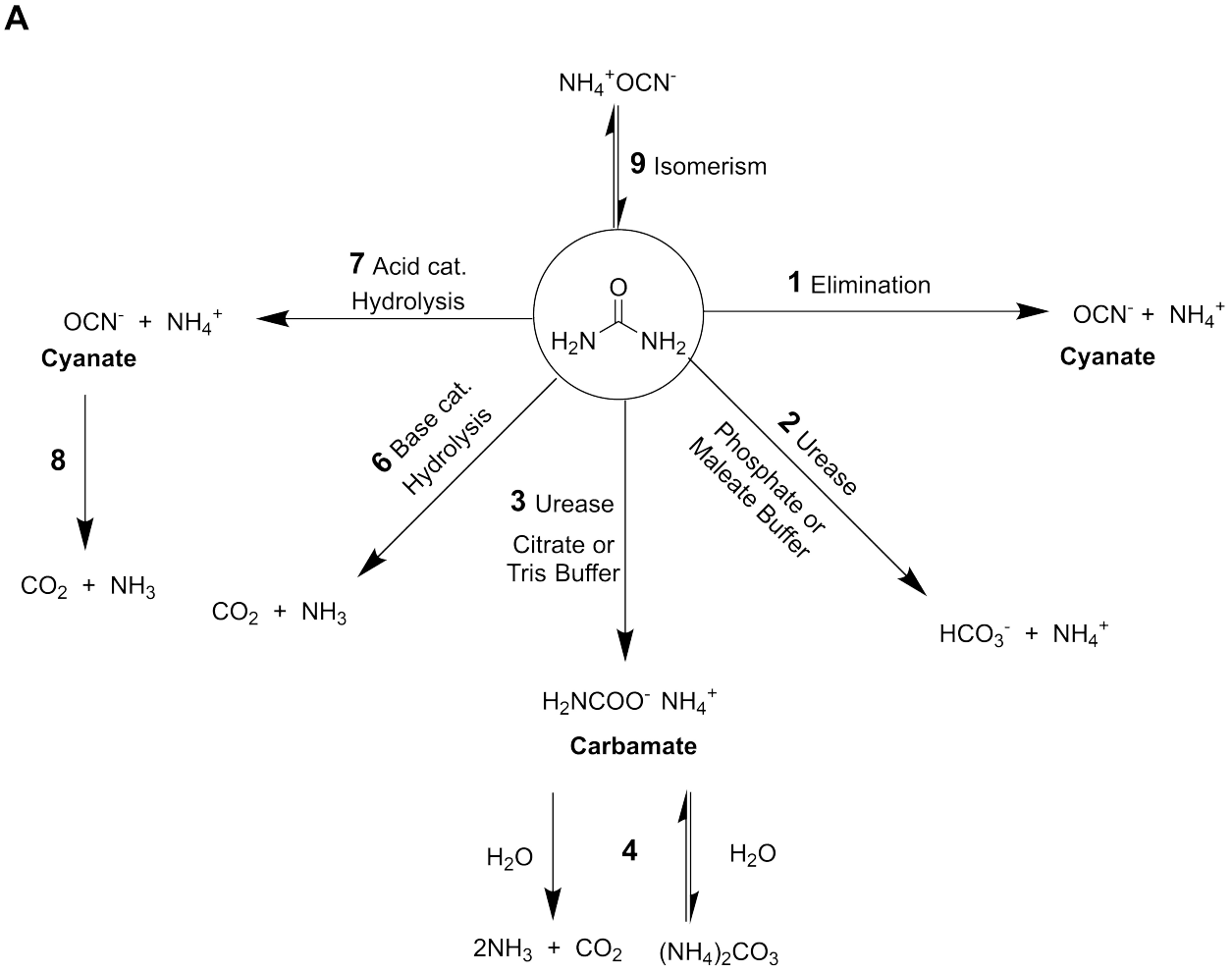


**Scheme 2.1:** Hydrolysis and elimination reactions involving urea.

Ammonium carbamate, although a formal product of urea hydrolysis, is unstable in solution and tends to revert to ammonia and carbon dioxide, Scheme 2.1 structure **4**, and undergo reversible hydration, Scheme 2.1 structure **4**, according to the Equations [108]:

$$NH_2CO_2NH_4 \rightarrow 2NH_3 + CO_2 \tag{2.1}$$

$$NH_2CO_2NH_4 + H_2O \rightarrow (NH_4)_2CO_3 \tag{2.2}$$

Ammonium carbamate is an intermediate in the production of urea from ammonia and carbon dioxide [109].

Wen and Brooker performed Raman experiments of solutions of ammonium carbonate, ammonium bicarbonate, ammonium carbamate, and ammonium chloride with sodium carbonate to investigate the equilibrium between ammonium carbonate, ammonium bicarbonate, and ammonium carbamate in solution [110]. Solutions of ammonium carbonate and bicarbonate were both found to have equilibrium amount of ammonium carbamate in solution and no urea was found in the solution of ammonium carbamate even at high temperatures, Scheme 2.1 structure **5**. The equilibrium in Equation 2.3 demonstrates how these species are related in solution.

$$HCO^-_{3(aq)} + NH_{3(aq)} \rightleftharpoons CO^{2-}_{3(aq)} + NH^+_{4(aq)} \rightleftharpoons H_2NCOO^-_{(aq)} + H_2O_{(l)} \tag{2.3}$$

Carbamic acid is a salt of ammonia and carbonic acid. It is unstable in solution and hydrolyzes to form carbon dioxide and ammonia [110].

In the absence of urease, urea in water will hydrolyze to form either $NH_3$ and $CO_2$ or cyanate and $NH_4^+$, Scheme 2.1 structure **6** and Scheme 2.1 structure **7**, depending on the pH [111–113]. The $OCN^-$ formed in solution can undergo further conversion, Scheme 2.1 structure **8**, to form carbon dioxide and ammonia [41, 43, 111, 113, 114]. At neural pH, urea isomerizes and is in equilibrium [41, 42] with $NH_4^+CN^-$, Scheme 2.1 structure **9**.

### 2.4.2 Electro-oxidation

Urea, can be electrochemically oxidized. Products of electro-oxidation depend on multiple factors including: anode potential, identity and composition of the electrolyte, urea concentration, pH, temperature and anode material.

Literature on the behavior of urea on gold electrodes is limited to adsorption studies and no study dedicated to the products, if any, of urea oxidation on gold has been performed to our knowledge. Review of the literature will therefore be limited to electrochemical reactions of urea involving other noble metals, for example platinum.

Bezerra concluded that in the presence of platinum and acidic media urea is oxidized to $CO_2$ and $N_2$ above 0.54 V vs Ag/AgCl [12]. In neutral media, $CNO^-$ and $[N_2O_2]^{2-}$ are produced at lower potentials, up to 0 V vs Ag/AgCl, and $NO_2$ and $NO_3^-$ are produced at more positive potentials. Using DEMS, Bolzan and Iwasita found that $CO_2$, $N_2$ and nitrogen oxides were oxidation products of urea on platinum in phosphate buffer and Krebs-Ringer bicarbonate solution, a mixture of several salts dissolved in water to produce a solution that is isotonic relative to animal body fluids, at potentials above +0.49 V vs Ag/AgCl [13]. Osetrova and Skundin investigated the effect of the anion on the anodic oxidation of urea. In solutions of neutral sulfate, fluoride, chloride and bromide both $N_2$ and $NO_3^-$

were produced [115]. The oxidation of urea in the presence of chloride may occur indirectly through hypochlorite formation at the electrode surface.

The study of the adsorption of urea to a polycrystalline gold surface will be furthered by investigation of its adsorption as a function of applied potential. The adsorption of likely products of urea hydrolysis and electro-oxidation will also be investigated.

# Chapter 3

# Materials and Methods

## 3.1 Materials

Reagents are all ACS grade unless otherwise stated. Ammonium carbamate ($NH_2CO_2NH_4$), ammonium chloride ($NH_4Cl$), ammonium fluoride ($NH_4F$), biuret ($NH(CONH_2)_2$), hydrofluoric acid (HF, 48 %), hydrogen peroxide ($H_2O_2$, 30 %), nitric acid ($HNO_3$), potassium chloride (KCl), sodium cyanate (NaOCN, 95 %), sodium fluoride (NaF), sodium sulfate ($Na_2SO_4$), sodium sulphite ($Na_2S_2O_3$), sulfuric acid ($H_2SO_4$), tetrachloroaurate trihydrate ($AuCl_3HCl{\cdot}3H_2O$), and urea ($(NH_2)_2CO$) were all used as purchased. All solutions were either prepared in Milli-Q water (>18.2 M$\Omega$ cm$^{-1}$) or deuterium oxide (99.9 atom % D).

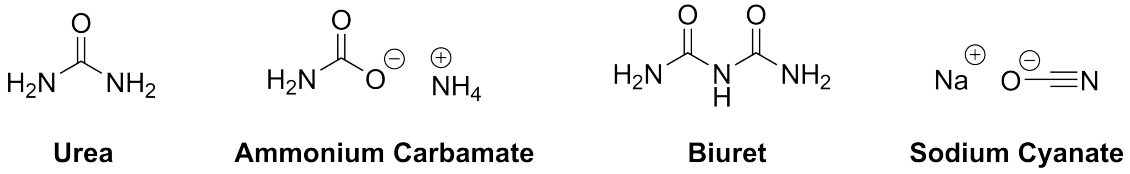


**Figure 3.1:** Structures of compounds relevant to spectroelectrochemical experiments.

## 3.2 Glassware

Prior to use all glassware was cleaned in a heated acid bath made from concentrated 3:1 $H_2SO_4$:$HNO_3$, thoroughly rinsed with MilliQ water and then left to soak in MilliQ water

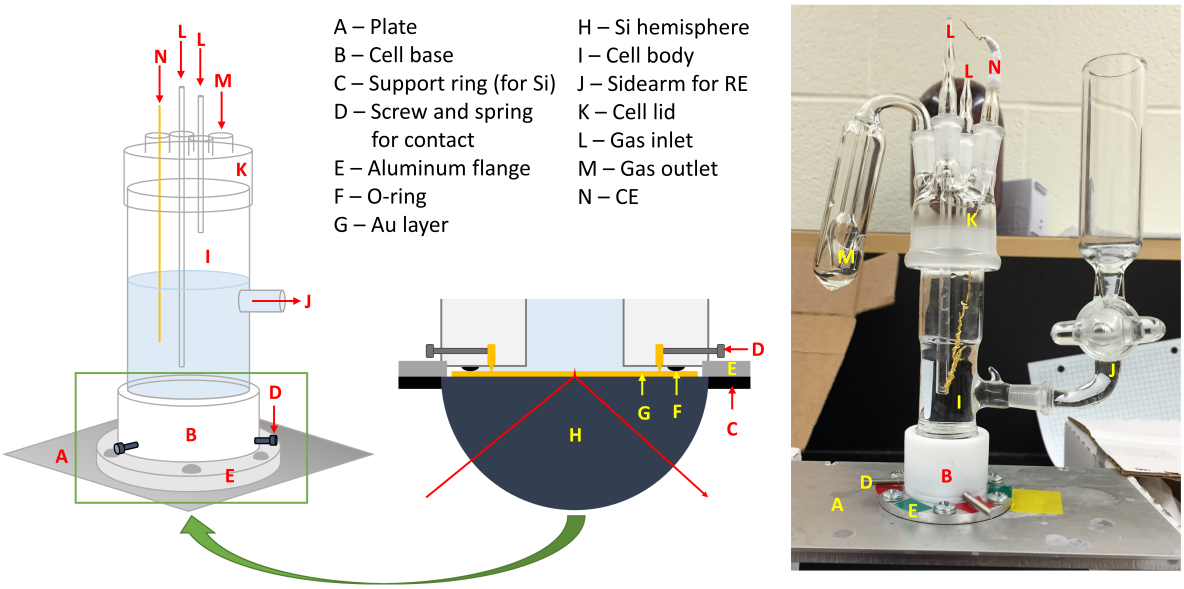


**Figure 3.2:** Scheme and picture of the spectroelectrochemical cell.

for a minimum of two hours. All teflon pieces and gaskets were cleaned in freshly made 4:1 concentrated sulfuric acid and 30 % $H_2O_2$.

### 3.2.1 Development of new spectroelectrochemical cell

The spectroelectrochemical cell used is a newly developed cell design based on a previous design in the group [116]. The original cell was three sections made of teflon that were held together by aluminum flanges. A sidearm attached to the body housed the reference electrode and ports for the counter electrode, two gas inlets and one gas outlet port were located in the lid. Each section was held together with six screws.

The new cell, colloquially referred to as the "Glass Castle", significantly improves on the old design. The cell base is made of teflon and the body and lid are made of glass. Compared to the old design, assembly is easier as the glass cell body is screwed into the large threads

in the cell base and the assembly is finished by placing the lid on the cell, eliminating the need for multiple aluminum flanges and screws. The cell seal is higher quality and eliminates the irreproducibility of positioning the flanges on the old base, body and lid, each which need to be removed before cleaning. The ports in the lid are made with ground glass joints which eliminates the need for screw-in ports, making assembly easier and allowing it to be purged of oxygen for electrochemistry experiments. Cleaning is easier as there is a smaller number of parts to clean and the cell is easily disassembled. A cell primarily made of glass is advantageous for three reasons; cleaning is easier, visual inspection of the inside of the cell is possible, and glass does not become distorted with prolonged use. A cell which is easier to assemble results in reproducible data.

Contact with the conductive gold surface is made using a screw and gold pin in the cell base and assembly of the cell base to the plate occurs through an aluminum flange and screws. The pins are an improvement on the original design as they provide high surface area for contact and do not scratch the gold layer, resulting in poor electrical contact. A gasket in the cell base provides the seal on the gold film to prevent solution from leaking into the purged spectrometer chamber and onto the delicate optical mirrors. Leaking solution can damage the optical mirrors and introduce stubborn water vapor into the chamber that results in peaks from the vibrational spectrum of water. The plate is machined to fit on the top of the ATR box which allows *ex situ* assembly of the cell, making it possible to test for leaks outside of the spectrometer. The total volume of the cell is approximately 20 mL. A scheme and picture of the Glass Castle can be seen in Figure 3.2.

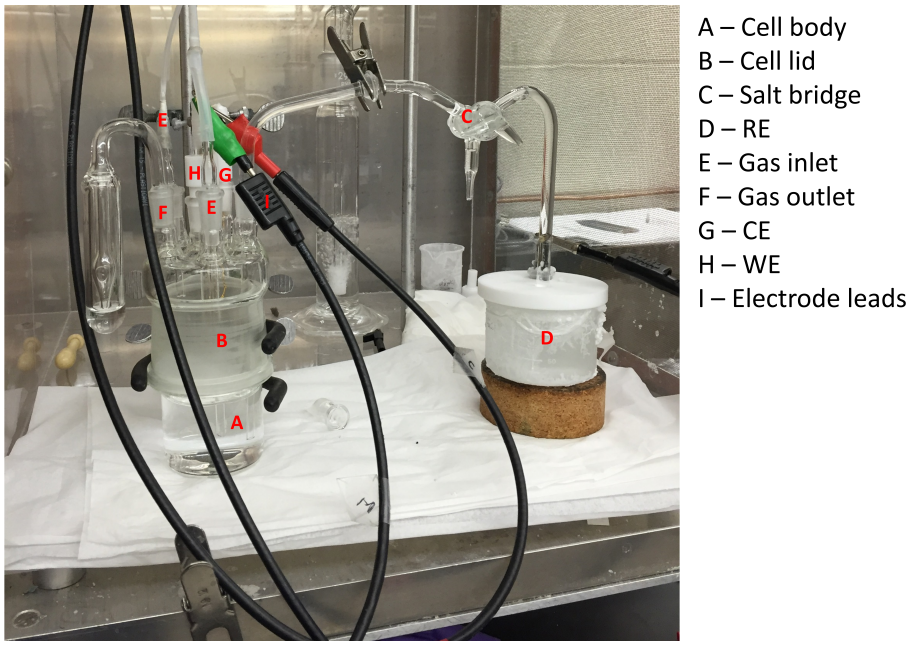


**Figure 3.3:** Benchtop electrochemical cell for CV and DC measurements.

### 3.2.2 Benchtop eletrochemical cell

The electrochemical cell used in all benchtop measurements is a standard glass cell with ports for the purge gas inlets and outlet, electrodes and salt bridge and can be seen in Figure 3.3. The total volume of the cell is 100 mL. A coiled gold wire was used as the counter electrode (CE) and an Ag/AgCl (saturated KCl) reference electrode (RE) is used. All solutions were purged with $Ar_{(g)}$ prior to use for 30 mins. Potential was controlled using a HEKA PG 590 potentiostat. A Stanford Research Systems Model SR830 DSP lock-in amplifier was used for differential capacitance experiments.

The working electrode (WE) was a polycrystalline gold bead for benchtop electrochemistry. Both gold counter and gold bead working electrodes are flame annealed prior to use, and the gold bead working electrode is electrochemically cleaned in 50 mM NaF. The WE and CE are made using 0.5 mm gold wire (Alfa Aesar, 99.9985%).

## 3.3 Electrochemistry

Two different types of measurements were performed, cyclic voltammetry (CV) and differential capacitance (DC). In cyclic voltammetry, the current is measured as a function of the applied voltage, E, by cycling between $E_1$ and $E_2$.

A three electrode cell is used, with the potential difference being applied between the working electrode and reference electrode. The RE used in an Ag/AgCl electrode filled with a saturated KCl solution. The CE is a coiled gold wire and the working electrode is either a gold bead electrode or a thin gold layer deposited on a silicon hemisphere.

CV was done at a relatively slow scan rate (20 – 50 mV/s). A scan rate of 50 mV/s was used when performing benchtop experiments and a scan rate of 20 mV/s was used for electrochemical cleaning of the gold layer. A slower scan rate was used to mitigate excessive oxygen and hydrogen evolution which can lead to destruction of the fragile gold layer.

In DC measurements, the capacitance of the surface is measured as a function of potential and allows measurement of non-Faradaic processes occurring at the WE, such as the adsorption of molecules, that do not involve the transfer of electrons and is governed by Equation 3.1, where C is the differential capacitance, $\epsilon$ and $\epsilon_o$ are the relative and vacuum permittivities, A is the electrode area, and d is the distance between the two planes of charge, in this case the electrode and the plane of closest approach of the electrolyte ions.

$$C = \frac{A\epsilon\epsilon_o}{d} \tag{3.1}$$

As neutral molecules adsorb to the surface and replace the charged electrolyte ions the capacity decreases.

DC measurements were done at a slower scan rate (5 mV/s) and are only performed in the double-layer region where no Faradaic processes are occurring.

CV data is presented as a plot of current density, j ($A/cm^2$), as a function of potential, E, and differential capacitance data is presented as a plot of capacitance, C ($\mu F/cm^2$), as a function of potential, E.

## 3.4 Infrared spectroscopy in transmittance and absorbance modes

All infrared (IR) spectra were obtained using a Nicolet Nexus 870 FT-IR or Bruker Vertex 70 FT-IR spectrometer. Transmission experiments were performed using a house made transmission cell in which a thin 25 $\mu$m gasket is sandwiched between two $CaF_2$ windows with an inlet and outlet for filling. Absorbance measurements were collected in the ATR configuration using an unmodified silicon hemisphere from Harrick Scientific Products with an incidence angle of 70°.

Infrared spectroscopy, one of the most common spectroscopic techniques, is useful for providing information on molecular structure. Spectra are collected from 4000–400 $cm^{-1}$ and investigates molecular bending and stretching vibrations. Infrared spectroscopy provides a "fingerprint" for a molecule, as no two non-identical molecules will provide the same spectra. Each type of bond is found only in a small frequency range of the spectrum and only vibrational modes that have a changing transition dipole moment (TDM) will be observed.

### 3.4.1 Data treatment in IR spectroscopy

All spectra were subtractively normalized as in Eq. 3.2, where $S_{sample}$ represents the sample spectrum and $S_{Ref}$ represents the reference spectrum:

$$\frac{\Delta S}{S} = \frac{S_{Sample} - S_{Ref}}{S_{Ref}} \tag{3.2}$$

Resultant spectra are interpreted as follows. Downward going peaks indicate an increase in the number density of the absorbing species and/or a reorientation of the molecule such that the TDM of a given vibrational mode has become more aligned with the electrode surface normal. Upwards going peaks indicate a decrease in the number density of the absorbing species and/or reorientation of the molecule such that the TDM of a given vibrational mode has become less aligned with the electrode surface normal.

## 3.5 Surface Enhancement in Infrared Spectroscopy

Surface enhancement is a process by which molecules adsorbed on a metal surface provide more intense infrared absorption than in the absence of metals. The initial discovery of this effect occurred in the measurement of aromatic carboxylic acids adsorbed on vacuum deposited gold and silver films. SEIRAS can be observed in transmission, external reflectance and ATR modes [117, 118].

Film morphology is critical to the surface enhancement effect [119–121]. Hartstein *et al.* demonstrated the importance of film thickness by studying the enhancement effect of different Ag film thicknesses (from 4–14 nm) on the absorption spectrum of p-nitrobenzoic

acid [119]. The intensity increased with increasing film thickness up to 10 nm. At 14 nm, the signal drops drastically due to coagulation of the metal islands on the film. Layers which give rise to surface enhancement are not continuous but consist of islands smaller than the wavelength of incident radiation [120]. Therefore, the roughness of the film is important [122].

Multiple studies have led to the consensus that two mechanisms contribute to surface enhancement: an electromagnetic (EM) and a chemical mechanism [117, 123–130]. Estimation of the field enhancement from the EM mechanism in the IR region is 10-fold or less and cannot account for the up to 1000 fold increase observed [123, 131]. Discussion of the EM mechanism of surface enhancement is normally done in terms of SERS but the same mechanism is expected for SEIRAS [119, 124, 125]. Metal particles of a particular size generate their own electric field when exposed to electromagnetic radiation of a wavelength larger than that of the particle [132–134]. This occurs through polarization of the particle by excitation of collective electron resonance or localized plasmon modes. This is demonstrated in Figure 3.4, where the induced dipole is denoted by $p$. The local EM field generated by the metal particle is approximately an order of magnitude stronger than the incident EM field [123]. Simulation have indicated that the shape of the particle also plays an important role. Anisotropic particles which are elongated parallel to the surface lead to greater degrees of surface enhancement than spherical particles [135]. Thin films, islands, and rough films can all be approximated as particles on a film. Simulations revealed that interaction between metal island play an important role and that the best enhancement is received when particles are close together but not touching [136]. The enhanced EM field decays quickly as the distance from the metal surface increases therefore the effect is sensitive to molecules adsorbed

near the surface [132–134, 134]. The enhancement diminishes within approximately 5 nm from the metal surface [117, 126, 136, 137].

In terms of SERS, noble metals like gold, silver and copper give rise to significant enhancement, while it is hardly observed or is weak on transition metals [132, 133]. EM calculations predict that enhancement using transition metals in the IR region should occur as strongly as with coinage metals owing to the similarity between the dielectric constants of the metals in the infrared region [120]. Early experiments demonstrated negligible surface enhancement effects with vacuum deposited films of transition metals [138, 139] but subsequent experiments revealed that surface enhancement does occur on many transition metal films such as Fe, Pt, Sn, Pb, Pd, Pt supported on Au films, Ir, Ni, Rh, Ru and Pt-Fe alloys [121, 140–150].

Measurement of adsorbed molecules on metal particles occurs through perturbation of the optical properties of the metal film. Molecules adsorbed to the surface exist in the localized electric field of the metal particle. As the probability of an IR vibrational transition occurring is proportional to $|E|^2$, the metal surface acts as an amplifier of the vibrational transition. These oscillating dipoles induce dipoles in the metal particles resulting in a change in the dielectric function of the particle [132–134]. Therefore, these vibrations are observed as changes in the transmittance or absorbance of the metal film.

As with infrared absorption spectroscopy in the solution phase surface selection rules exist that govern which vibrations can be observed when molecules are adsorbed to a surface. Osawa *et. al* studied the adsorption of the potassium salt of p-nitrobenzoic acid on a smooth bulk silver surface using infrared reflection-absorption spectroscopy (IRRAS) and SEIRAS [151]. As the orientation of the adsorbed molecule and the resulting spectra are identical for

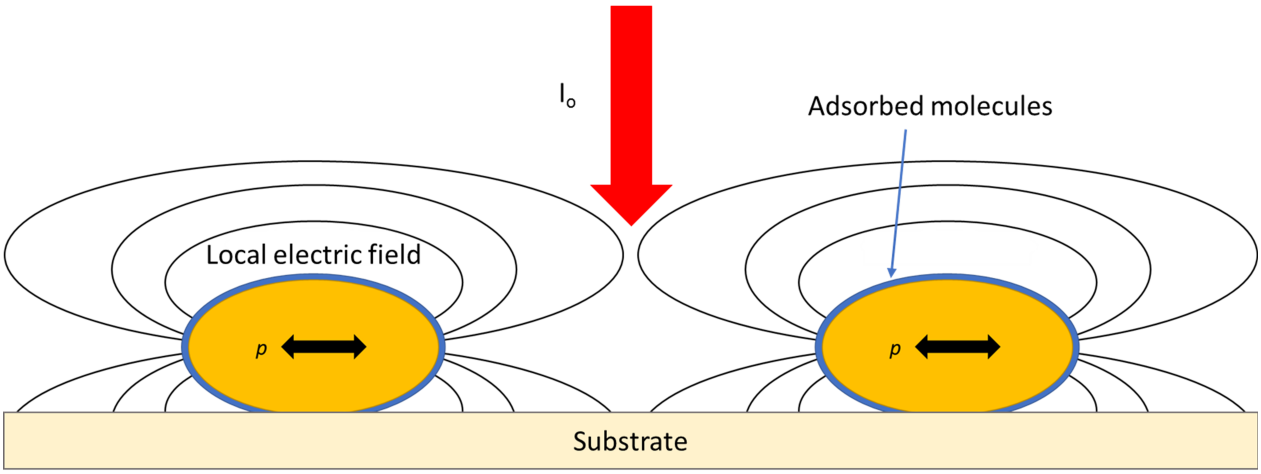


**Figure 3.4:** Localized electric field around two metal particles. Adapted from [138].

both techniques, the selection rules are the same. Only vibrations with a transition dipole moment normal to the surface are IR-active [152].

The adsorption configuration of molecules to a surface contribute to signal enhancement. Molecules that are all adsorbed in the same configuration, with dipole oscillations normal to the surface, should have enhancement three times more intense than those with random orientations [123]. In terms of chemical mechanisms, chemisorbed molecules exhibit larger enhancement than physisorbed molecules. Chemisorption changes the polarizability of a molecule and vibrations of strongly polarized groups generally result in larger enhancement compared to other groups due to donor-acceptor interactions in the molecule [127]. Charge oscillations between the molecular orbitals of adsorbed molecules and those of the metal may increase the adsorption coefficient of the adsorbate, based on theoretical calculations [153, 154]. Adsorption of CO on iron films de-

posited on MgO(001) occurs with a very asymmetric peak shape that is well simulated using the charge-transfer mechanism [140]. Asymmetric band shapes can be explained using the EM mechanism as well therefore a chemical mechanism as the origin of the asymmetric band shape are still open to discussion [121].

## 3.6 Gold layer preparation and cleaning

SEIRAS-active gold layers were prepared by electroless deposition onto a Si hemisphere using a plating solution. The Si hemisphere was first polished using 3 $\mu$m then 0.5 $\mu$m diamond polishes and thoroughly rinsed. The exposed surface is then cleaned for 3 minutes using ammonium fluoride before being placed in a hot water bath at 55°C. A fresh plating solution made up of 2% HF, $AuCl_3$·HCl, $Na_2SO_4/Na_2S_2O_3$ buffer and $NH_4Cl$ is added over a period of one minute by adding 1 mL of solution, then removing 0.5 mL, then adding another 0.5 mL and repeating until none remains. The reaction is quenched with Milli-Q water. The gold deposition takes place by the oxidation of Si through the following reaction [155] at 55 °C :

$$3Si_{(s)} + 18F^-_{(aq)} + 4AuCl^-_{4(aq)} \rightarrow 3SiF^{2-}_{6(aq)} + 4Au_{(s)} + 16Cl^-_{(aq)} \tag{3.3}$$

Once rinsed, the Si hemisphere is assembled in a house made spectroelectrochemical cell.

Figure 3.5 shows a gold layer on the Si hemisphere before assembly in the spectroelectrochemical cell. A good gold layer is shiny, yellow and consistent in appearance. Indications of a substandard gold layer which may fail are dark areas of thinning gold, bright spots with dark holes in the center, areas of white discoloration in thinning areas and holes where there

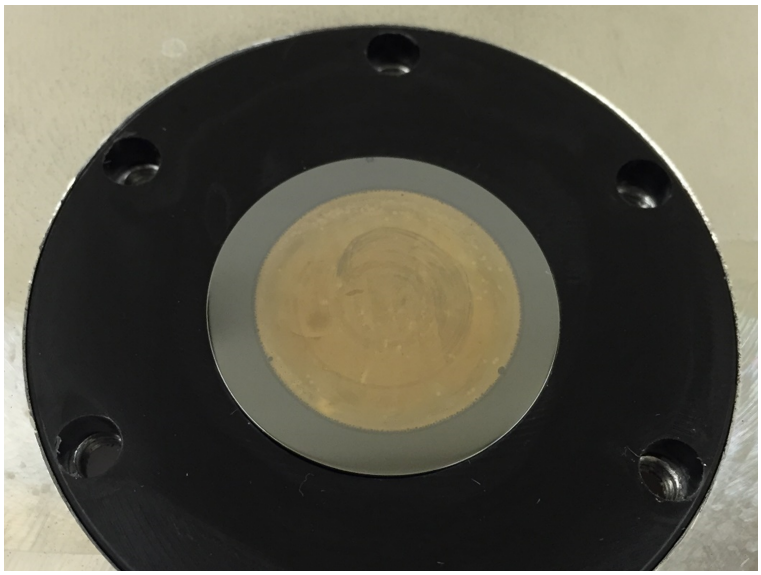

**Figure 3.5:** Gold layer before assembly of spectroelectrochemical cell.

is evidently no gold. Only layers that do not exhibit any of these characteristics, or those in which these areas fall outside the seal created by the o-ring, are used.

Prior to use for SEIRAS experiments the layer is electrochemically cleaned in 50 mM NaF by cycling the potential between - 0.5 V and 0.6 V vs. Ag wire until the resulting CV, see Section 3.3, is stable. A stable CV of the thin gold layer in 50 mM NaF is shown in Figure 3.6.

## 3.7 Spectroelectrochemistry

All spectra were obtained using a Bruker Vertex 70 FT-IR spectrometer using a VeeMAX II ATR accessory (Pike Technologies) in the ATR configuration. The house made electrochemical cell, the "Glass Castle", is set up on the infrared spectrometer and is used to perform all potential dependent studies. The working electrode is a thin gold layer and preparation is outlined in Section 3.6. All electro-oxidation was done in the presence of 50 mM supporting

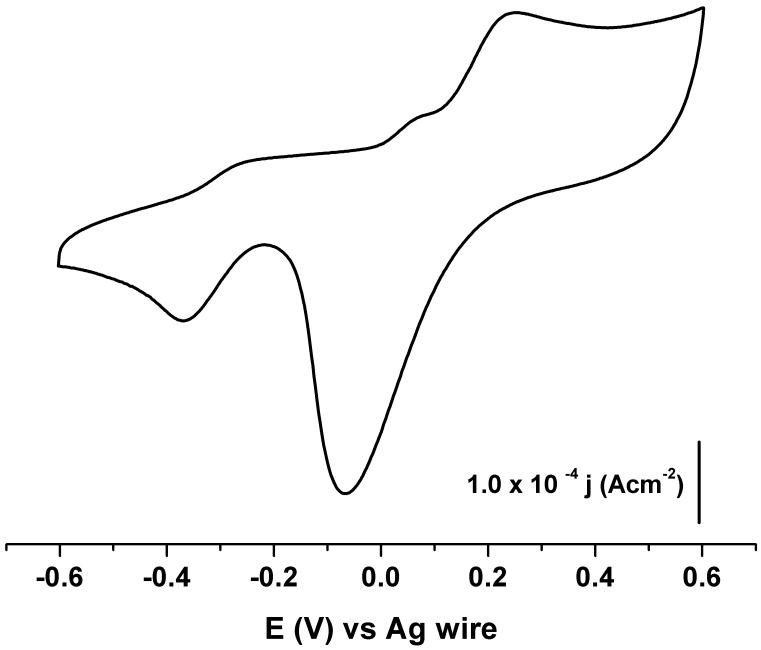


**Figure 3.6:** Stable CV of the gold layer in 50 mM NaF during electrochemical cleaning. Scan rate: 20 mV/s.

electrolyte, NaF, in $D_2O$ or $H_2O$ and the potential was controlled using a HEKA potentiostat. All spectra were treated as with transmission and absorbance experiments described in Section 3.4.1.

In the infrared experiments the adsorption behavior of urea is studied in both $D_2O$ and $H_2O$. The $H_2O/D_2O$ peaks overlap with the NH/ND and $\nu$(CO) peaks of urea. Two peaks appear for $H_2O$: a broad peak centered around 3400 $cm^{-1}$ and a second centered around 1650 $cm^{-1}$. The 1650 $cm^{-1}$ band appears in the same region as CO stretching frequencies, by performing experiments in $D_2O$ the OH stretching vibration is shifted outside that region. The OD stretch of $D_2O$ appears around 1207 $cm^{-1}$, below the Si cutoff of $\sim$1250 $cm^{-1}$ [156]. The $D_2O$ bending vibrations shifts to lower wavenumbers and causes partial overlap with another region of interest around 2100 $cm^{-1}$. HOD appears at 1446 $cm^{-1}$ for solutions

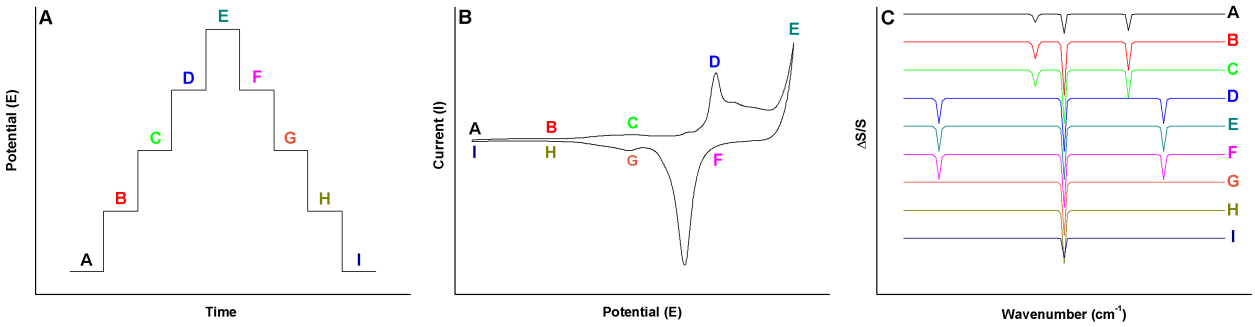


**Figure 3.7:** A) Potential sweep diagram, resulting B) cyclic voltammogram and C) difference spectra for spectroelectrochemical experiments. Letters indicate potential where difference spectra were obtained.

containing H and D atoms [156]. The combination of $H_2O$ and $D_2O$ experiments allows for both regions to be studied without interference. During experiments in $D_2O$ the reference electrode is filled with a solution of saturated KCl in $D_2O$.

Figure 3.7 shows the relationship between the potential waveform, A, the resulting CV, B, and the resulting spectra, C, for a theoretical SEIRAS experiment. Figure 3.7A demonstrates how the potential is changed as a function of time during the experiment: it is swept to a target potential and held while the IR spectrum is collected, the potential is then swept by another 100 mV interval, held and the IR measurement taken. This is repeated until the measurements are performed across the forward and reverse scans. Letters A–I indicate potentials where spectra are measured. Figure 3.7B represents a CV of the system with letters indicating the positions where the potential was held. Figure 3.7C represents the difference spectra that would result at each potential. These are compared by stacking the spectra from A–I which simplifies spectral interpretation.

Techniques described above, IR in absorbance and transmission modes, SEIRAS, CV and DC will be used to characterize the adsorption of urea on a polycrystalline gold bead and thin layer gold film electrodes.

# Chapter 4

# Results and Discussion

## 4.1 Electrochemistry of urea on a polycrystalline gold electrode

Electrochemistry was performed in a benchtop electrochemical cell to determine the behavior of urea on gold with applied potential. Initial characterization provides information on the regions of interest to be probed in spectroelectrochemical experiments.

In cyclic voltammetry there are two different regions of the voltammogram which provide unique information about the behavior of a molecule. The double-layer region (-0.8 – 0.9 V for gold in NaF and urea) provides information on the adsorption and change in configuration of a molecule on the electrode surface. This region ends at the onset of electrode oxidation, where there is a large increase in current and is the beginning of the region where oxidative processes are occurring at the electrode surface. In this region, the products formed are from the oxidation of species in the system, in this case urea, the solvent and the electrode.

Cyclic voltammograms in the double-layer and oxidation regions of urea in neutral solution are shown in Figure 4.1. In Figure 4.1A in the absence of urea (black line) produces a characteristic current response for a polycrystalline gold electrode. In the absence of urea,

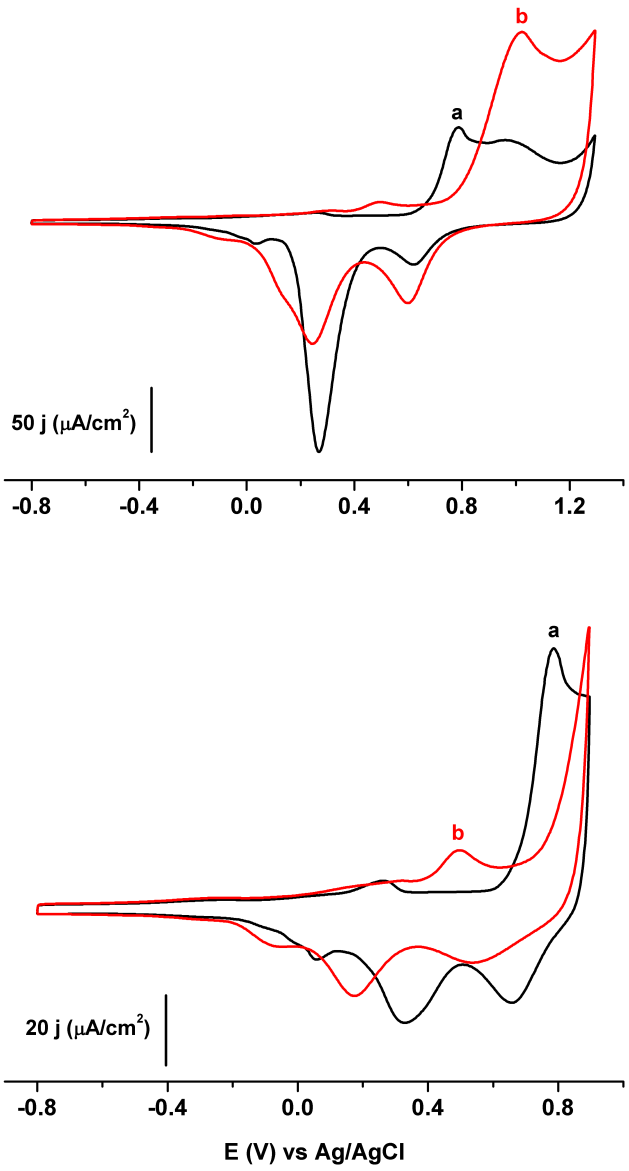


**Figure 4.1:** Electrochemical behaviour of urea in a benchtop electrochemical cell. A) In the oxidation region. B) In the double-layer region. (a): 50 mM NaF, black (b): 50 mM NaF + 20 mM urea, red.

peaks appear at 0.78 and 0.99 V in the forward sweep and are attributed to oxidation of polycrystalline gold. The increase in current at 1.16 V is from the oxidation of water which occurs through the following equation:

$$2H_2O_{(l)} \rightarrow O_{2(g)} + 4H^+_{(aq)} + 4e^- \tag{4.1}$$

Peaks at 0.63, 0.28 and 0.01 V in the reverse sweep are from the reduction of gold oxide formed in the forward sweep. In the presence of urea (red line) two peaks appear in the forward sweep at 0.50 V and 1.02 V. The peak at 0.50 V is due to the adsorption of urea on gold and the peak at 1.02 V is due to the concomitant oxidation of gold and urea. The increase in current above 1.14 V is indicative of oxygen evolution (Equation 4.1). In the reverse sweep three peaks appear at 0.61, 0.24 and -0.09 V. As these occur at potentials slightly more negative than those of gold reduction in NaF these belong to a combination of gold reduction with subsequent urea readsorption, indicating that urea does not adsorb on gold oxide.

For Figure 4.1B, in the presence of urea an increase in current appears in the range of 0.20–0.60 V with a peak at 0.50 V in the forward direction and peaks at -0.08, 0.17 and 0.54 V in the reverse sweep due to the reduction of gold oxide. Differential capacitance experiments provide information on the electrode surface. A decrease in capacitance after the addition of a new species indicates the species is adsorbing on the surface. Figure 4.2 shows the differential capacitance of the gold electrode in supporting electrolyte and in the presence of urea. In the forward sweep, the capacitance in the presence of urea becomes less than in the presence of NaF at -0.09 V therefore urea is adsorbing above this potential and

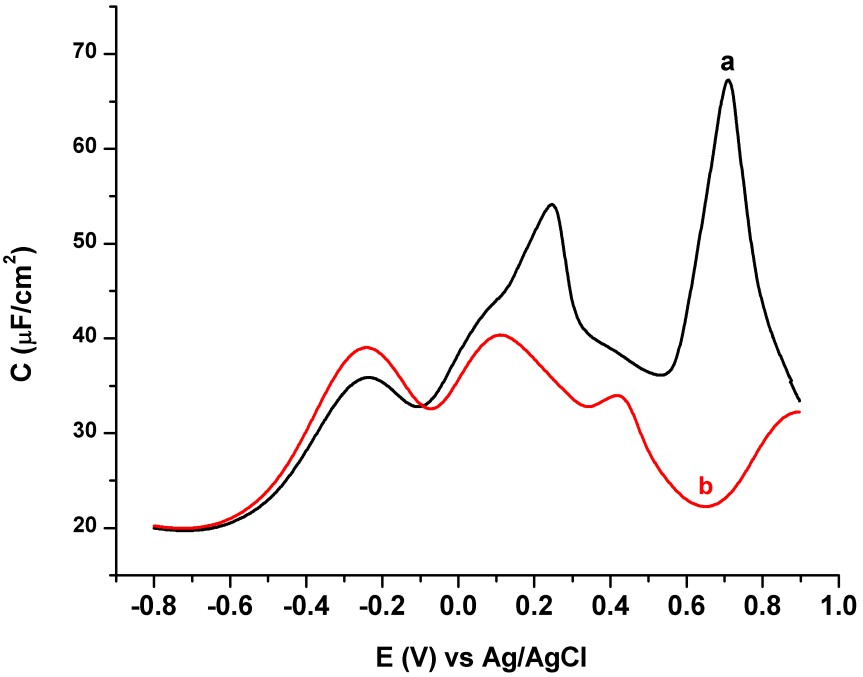


**Figure 4.2:** Differential capacitance in a benchtop electrochemical cell (Forward scan). (a): 50 mM NaF, black (b): 50 mM NaF + 20 mM urea, red.

is the process observed in the 0.10–0.50 V range of the forward sweep of Figure 4.1A in the presence of urea.

CV and DC experiments indicate interesting adsorption, desorption and possible rearrangements occurring in the range of potentials studied. Ideally spectroelectrochemical experiments should be performed from *ca.* -0.6 to 1.0 V to include regions where processes are occurring but avoid extremes where the onset of hydrogen and oxygen evolution are observed at -1.0 and 1.2 V, respectively, which may result in destruction of the gold layer. From electrochemical cleaning of the gold layer the limiting potentials should be -0.5 and 0.9 V as the onset of hydrogen and oxygen evolution occurs at less negative and positive potentials. The range of accessible potentials is enough to characterize the breadth of processes even with the limitations imposed by the fragility of the gold layer. The vertex at 0.9 V is positive enough to investigate the process with an onset at 0.7 V but a vertex of -0.1 V is not negative enough

to completely reduce the gold oxide and return the electrode to its original configuration. Direct comparison between the same potential in two different sweep directions is therefore not possible because the electrode surface is different as it remains partially oxidized in the cathodic sweep.

## 4.2 Solution phase urea in adsorption and transmission mode

Electrochemical results provide information on processes involving the transfer of electrons but cannot elucidate the process behind the electron transfer. Such processes include adsorption/desorption involving the transfer of electrons, oxidation and reduction reactions and changing orientation of an adsorbed molecule. It cannot provide information on molecular identity or structure therefore a complimentary technique is needed. Infrared spectroscopy provides information on the types of bonds present in a molecule as well as molecular identity if a reference spectrum is known. Changes in spectra as a function of potential can be directly linked to changes in the cyclic voltammogram and therefore identify which processes are occurring. Investigation of the infrared adsorption of free urea simplifies the SEIRAS peak assignments.

The infrared spectra of urea were collected in $H_2O$ and $D_2O$ to demonstrate the effect of substituting $D_2O$ for $H_2O$ on the vibrational frequencies of urea. The geometry of the ATR configuration is such that only the first few $\mu$ms beyond the window surface are sampled, reducing the effect of solvent absorption. Figure 4.3 shows the absorption spectrum of urea on uncovered Si in the ATR configuration in $H_2O$ and $D_2O$. The frequency of the $\nu$(CO)

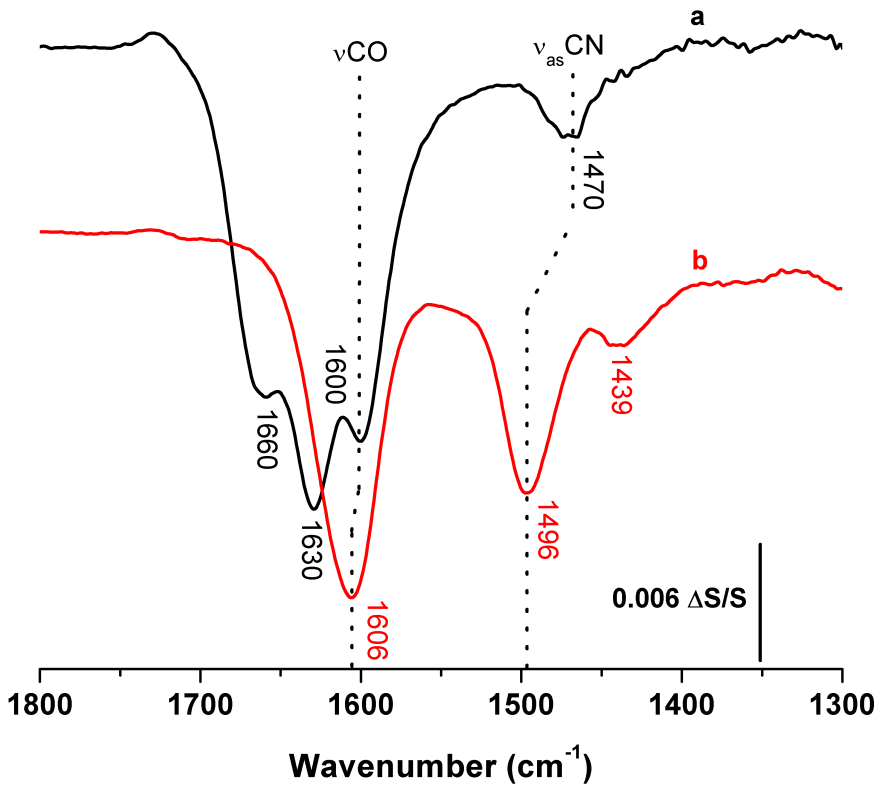


**Figure 4.3:** ATR-IR spectra of urea$_{(aq)}$. (a): Urea in $H_2O$, black (b): Urea in $D_2O$, red.

peak shifts from 1600 to 1606 $cm^{-1}$ and the $\nu_{as}$(CN) peak shifts from 1470 to 1496 $cm^{-1}$ upon deuteration due to coupling with the $ND_2$ bending vibrations [26].

Comparison with literature for solid urea yields the assignments summarized in Table 4.1 [26].

| $H_2O$ | | | $D_2O$ | | |
|---|---|---|---|---|---|
| | Literature [26] ($cm^{-1}$) | Fig. 4.3 ($cm^{-1}$) | | Literature [26] ($cm^{-1}$) | Fig. 4.3 ($cm^{-1}$) |
| $\delta_s NH_2$ | 1683 | 1660 | $\delta_s ND_2$ | 1223[a] | – |
| $\delta_{as} NH_2$ | 1625 | 1629 | $\delta_{as} ND_2$ | 1135[a] | – |
| $\nu_s CO$ | 1601 | 1600 | $\nu_s CO$ | 1608 | 1606 |
| $\nu_{as} CN$ | 1466 | 1470 | $\nu_{as} CN$ | 1490[b] | 1496 |

[a] Ref [85], Raman spectroscopy

[b] Estimated from Figure 6, Ref [26]

**Table 4.1:** Vibrational frequency assignments of solution phase urea in $H_2O$ and $D_2O$

The Si spectra of urea in $D_2O$ has two fewer peaks than in $H_2O$: those at 1660 and 1630 $cm^{-1}$ are no longer observable. This occurs as a result of isotopic substitution between the hydrogen and deuterium atoms which shifts these vibrational frequencies to below that of the Si cutoff around 1300 $cm^{-1}$. No evidence of NHD bending vibrations are observed between the regions for $\delta NH_2$ and $\delta ND_2$, 2450–3341 $cm^{-1}$ and 2601–2433 $cm^{-1}$ respectively, indicating the hydrogen atoms of urea are labile enough to quickly and completely substitute upon immersion in $D_2O$. Keuleers and Dessyn prepared deuterated urea molecules by dissolving their products in $D_2O$ and partially deuterated molecules were prepared by dissolving in appropriate ratio of $H_2O/D_2O$ [26]. Spectra in Figure 4.3 were collected using 1 M solutions

whereas the gold SEIRAS experiments are done at 0.01 M. The $NH_2$ and NH vibrations are not expected be observed for SEIRAS $D_2O$ experiments because of rapid substitution of $H_4$-urea at a much lower concentration. It is worth noting that the percentage of hydrogen from urea in a SEIRAS experiment is approximately 0.018 % and that of the experiments in Figure 4.3 is approximately 7 %, therefore no significant contribution from hydrogen is expected. The weak peak located at 1439 $cm^{-1}$ for urea in $D_2O$ in Figure 4.3 is due to the HOD bending vibration [156]. All other sources of hydrogen were minimized with thorough rinsing with $D_2O$, using a $D_2O$ reference electrode, sealing from atmospheric water and controlled monitoring of SEIRAS for $H_2O$ peaks. Finally, deuteration shifts the frequencies of the $\nu$(CO) and $\nu_{as}$(CN) vibrations to higher wavenumbers, from 1470 and 1600 $cm^{-1}$ to 1496 and 1606 $cm^{-1}$ respectively.

## 4.3 Adsorption behavior of urea on gold surfaces

The 1800–1500 $cm^{-1}$ region of the spectrum is important for the interpretation of urea adsorption on gold. The peaks in this region provide the information necessary to determine whether adsorption occurs through the oxygen atom or one or both nitrogen atoms and the orientation of the molecule with respect to the metal surface.

How a molecule adsorbs to a metal surface depends on many factors including crystal face orientation, surface coverage and applied potential. Different bonding modes give rise to different vibrational frequencies and the absence of a peak can provide as much information as the presence of one. Climent et al. have assigned bonding modes of urea on different crystal faces of platinum and rhodium based on this principle (see Table 2.5). Figure 4.4 restates

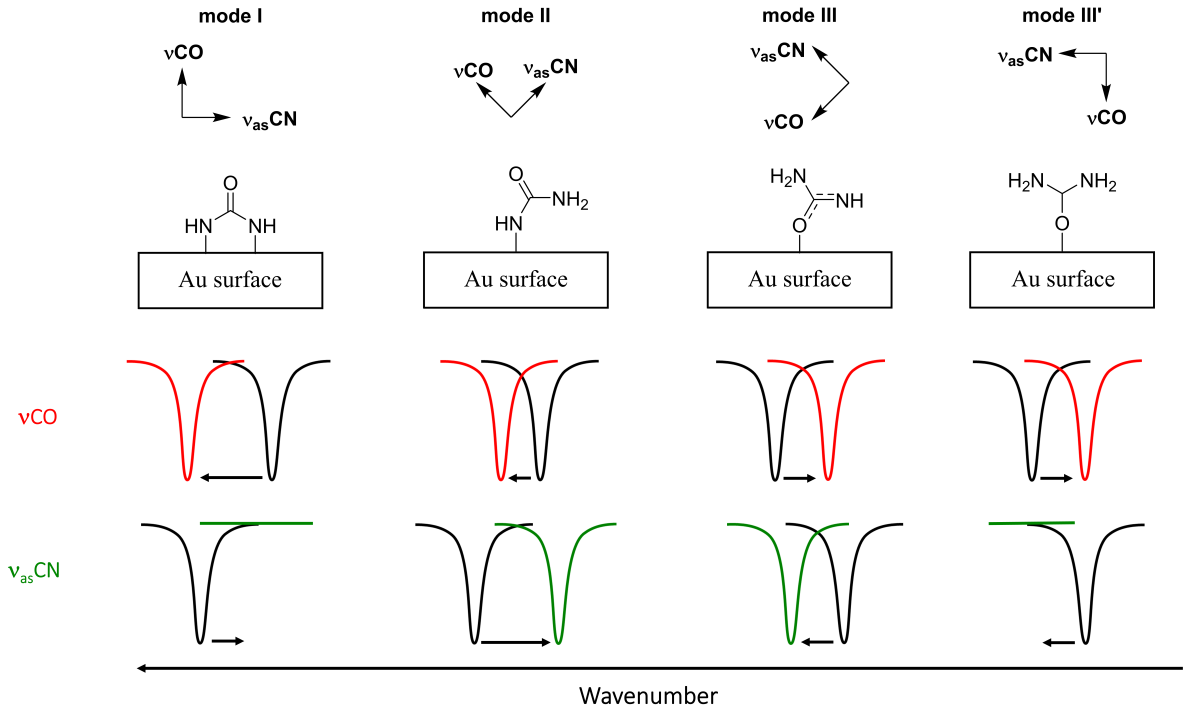


**Figure 4.4:** Different bonding modes of urea to metal surfaces, transition dipole moments, and representation of the shift in peak frequency upon adsorption for $\nu$(CO), red, and $\nu_{as}$(CN), green. From left to right: **mode I**) 2N-bonded; **mode II**) N-bonded; **mode III**) O-bonded (tilting); **mode III′**) O-bonded (normal).

the bonding modes from the literature review. Distinguishing between N-bonded, **mode I** and **mode II**, and O-bonded, **mode III** and **mode III′** urea can be done on the basis of the peak positions relative to those of free urea. In $H_2O$ solution, urea has multiple peaks at 1600 $cm^{-1}$ and a clearly resolved peak at 1470 $cm^{-1}$ (Figure 4.5A). Two peaks, $\nu$(CO) and $\nu_{as}$(CN), are reported in literature to be observed at 1655 and 1466 $cm^{-1}$ for free urea in $H_2O$ solution. Penland *et al.* used the position of these two peaks to determine the nature of urea adsorption in urea-metal complexes based on the shift in their positions relative to free urea [157]. When urea bonds through the nitrogen atom (or atoms) there is a reinforcement of the $\nu$(CO) double-bond character which causes a shift to higher wavenumbers (blue shift) and weakens the CN bond, shifting it to lower wavenumbers (red shift). The opposite occurs when urea bonds through the oxygen atom. This strategy has been employed to determine the bonding mode of urea in metal-urea complexes and has been employed to determine bonding modes on surfaces as well [5, 157, 158]. Comparing vibrational frequencies on surfaces to those in complexes does not guarantee an accurate assignment, but the study of metal-urea complexes by other methods such as Raman, UV and NMR spectroscopy and X-ray diffraction can provide complementary evidence for such assignments [159].

In adsorption experiments, the relative peak position compared to the free molecule is a result of the bonding mode and orientation. Surface selection rules dictate which molecular vibrations can be observed. On metals, only vibrations having a transition dipole moment component normal to that of the electrode surface can be observed [160]. The spectrometer uses p-polarized light which is polarized parallel to the plane of incidence and thus normal to the metal surface therefore only vibrations with a component matching the orientation of the polarization can be observed. The expected effect of the different urea adsorption

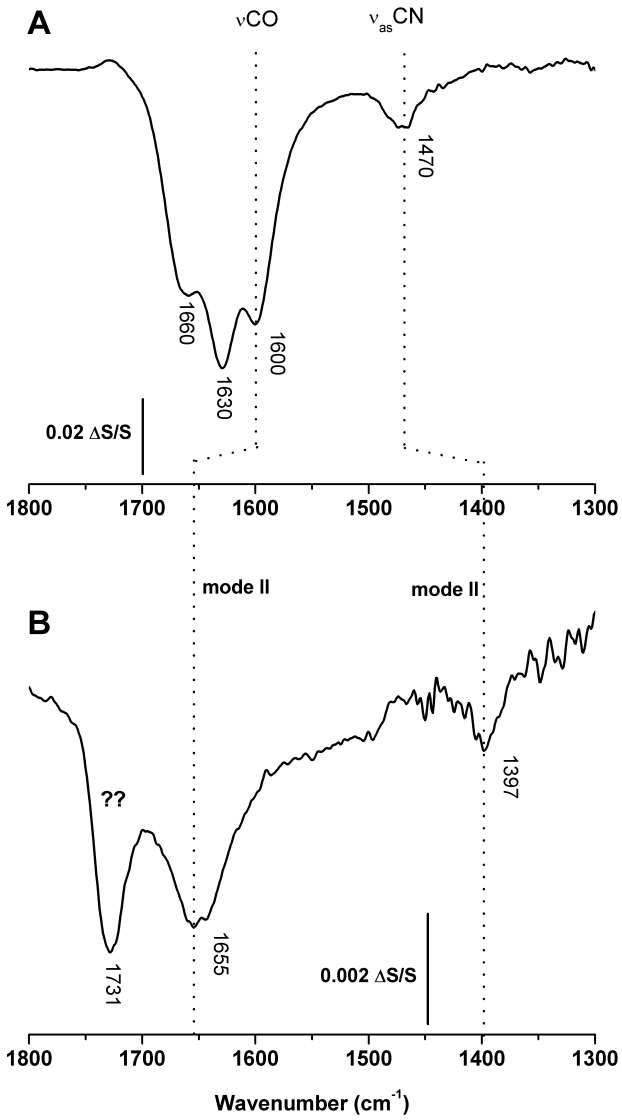


**Figure 4.5:** A) ATR spectra of urea and B) ATR SEIRAS spectra of urea adsorption on gold. In $H_2O$ based electrolyte.

| Metal | Sc | Mn | Co | Cu | Zn |
|---|---|---|---|---|---|
| Average M-O-C bond angle (°) [161] | 135.6 | 134.4 | 131.6 | 131.0 | 131.6 |

**Table 4.2:** Metal-O-C bond angles in some early solid crystalline transition metal-urea complexes

modes on $\nu$(CO) and $\nu_{as}$(CN) compared to free urea are summarized in Figure 4.4. The $\nu_{as}$(CN) is not observed in **mode I** as the transition dipole moment for the $\nu_{as}$(CN) stretch is parallel to the electrode surface and not observable [8]. If a high wavenumber $\nu$(CO) and a low wavenumber $\nu_{as}$(CN) are observed compared to free urea then adsorption occurs through a single nitrogen atom as the double bond character of $\nu$(CO) is reinforced but the $\nu_{as}$(CN) is still observable (**mode II**). Adsorption through two nitrogen atoms, **mode I**, shifts the $\nu$(CO) to even higher wavenumbers than adsorption through a single nitrogen atom but should not provide a signal for the $\nu$(CN) bond. Similarly, with O-bonded urea a single peak for $\nu$(CO) should be observed when urea is adsorbed normal to the surface (**mode III′**), however, if the molecule is tilted with respect to the metal surface $\nu_{as}$(CN) is observed (**mode III**) [9]. Lebioda reports the M-O-C bond angles in solid crystalline metal-urea complexes are far below 180° [161]. Bond angles for some urea-metal complexes are tabulated in Table 4.2. Therefore O-bonded urea with the $\nu$(CO) bond perpendicular to the surface, **mode III′**, is not expected. Urea has been shown to be sensitive to crystal face orientation therefore if urea adsorbs in multiple configurations peaks associated with each mode would be visible in the resulting spectrum and in a case where the metal surface is polycrystalline multiple bonding modes are possible [7–11, 38].

SEIRAS spectra of urea adsorption on gold in $H_2O$ is shown in Figure 4.5B. Three peaks are observed on gold at 1731, 1655 and 1397 $cm^{-1}$ and compared to free urea (Figure 4.5A), the $\nu_{as}$(CN) vibrational mode shifts from 1470 $cm^{-1}$ in solution to 1397 $cm^{-1}$ upon adsorption on gold and the $\nu$(CO) vibrational mode shifts from 1600 $cm^{-1}$ to 1655 $cm^{-1}$. A $\nu$(CO) shift to a higher wavenumber and $\nu_{as}$(CN) shift to a lower wavenumber indicates urea is adsorbed through a nitrogen atom. The presence of a weak $\nu_{as}$(CN) peak at 1397 $cm^{-1}$ indicates urea is bonded through a single nitrogen atom (**mode II**). The peak at 1731$cm^{-1}$, which has no analogous vibration in solution, could be from the $\nu$(CO) of urea adsorbed through two nitrogen atoms (Figure 4.4A) or the adsorption of a spontaneously formed urea decomposition product. This peak is unexpected and considerable effort was made to determine if it arises from a carbonyl-containing product from various known reactions involving urea.

## 4.4 Investigation of urea decomposition products

Scheme 4.1A shows the likely breakdown products of urea. Hydrolysis products of urea include ammonium carbamate, ammonium ion and bicarbonate when in the presence of urease at various pHs [107]. Although many of these reactions require elevated temperature or pressure to drive the reaction metal surfaces are known to catalyze simple reactions therefore these products were investigated. Hydrolysis conditions in the absence of urease produce ammonium ion, bicarbonate and ammonium carbamate at a slow rate (Scheme 4.1 structure **A** and Scheme 4.1 structure **B**). The ammonium carbamate formed in Scheme 4.1 structure **B** further hydrolyzes to form ammonia and carbon dioxide or ammonium carbonate, Scheme 4.1 structure **C** and Scheme 4.1 structure **D**. In the absence of urease, an elimination reaction

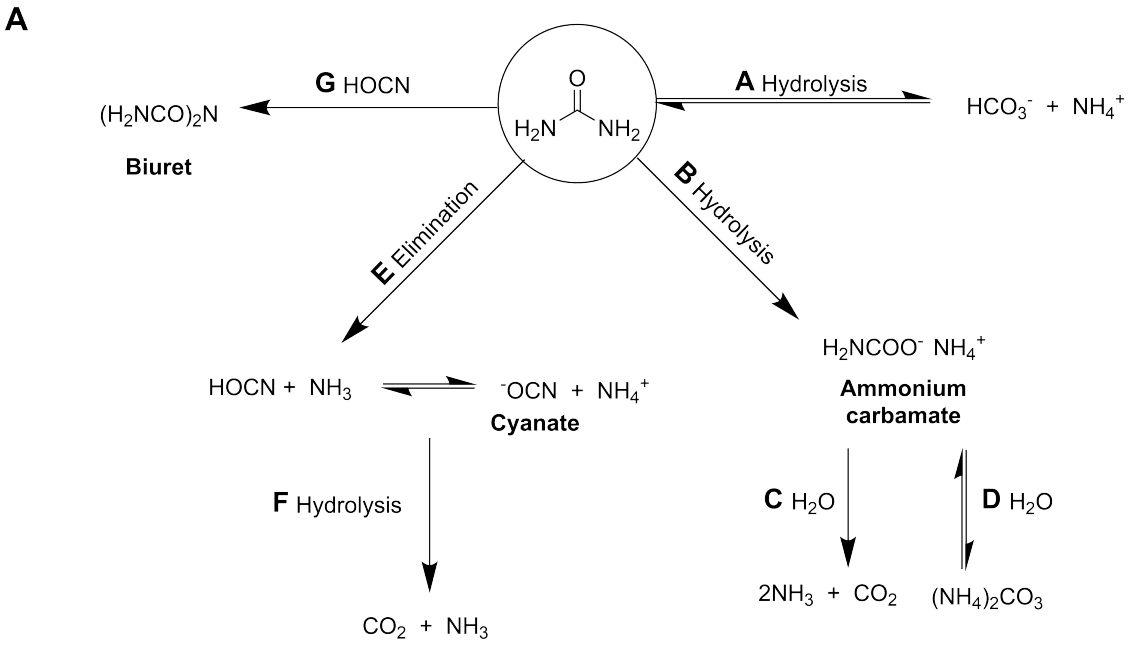


**Scheme 4.1:** Urea decomposition pathways

to form cyanate and ammonium ions is preferable to hydrolysis (Scheme 4.1 structure **E**) [106]. Elimination is preferable to hydrolysis in solution due to favorable hydrogen bonding interactions between urea and hydrogen from a single water molecule in the intermediate [105]. Urea can decompose to form $NH_3$ and HNCO in solution, which exists in equilibrium with $OCN^-$ and $NH_4^+$, Scheme 4.1 structure **E**, and at low concentrations HNCO hydrolyzes to form $NH_3$ and $CO_2$ (Scheme 4.1 structure Scheme 4.1 structure **F**) [42]. Cyanate formed from **E** can undergo hydrolysis, Scheme 4.1 structure **F**. In the presence of HNCO and elevated temperatures biuret can form (Scheme 4.1 structure **G**) [162]. Scheme 4.1B shows the equilibria which exists between ammonium carbamate, ammonium carbonate and ammonia and bicarbonate in solution [110].

To determine whether the peaks observed in Figure 4.5 are from processes in Scheme 4.1 experiments were performed using suspected urea reaction products. These products include biuret, cyanate, ammonium, carbon dioxide, ammonium carbamate and carbonate but those without carbonyl moieties such as ammonium and carbonate were not investigated. Spectra of $CO_2$ transmission and adsorption are not included as $CO_2$ is known to not adsorb on gold [163]. Figure 4.6 shows the transmission spectra (Figure 4.6A) and the SEIRAS spectra on gold (Figure 4.6B) of the likely breakdown products of urea which contain a carbonyl group.

Figure 4.6B shows the urea decomposition products adsorbed on gold. From the transmission data, Figure 4.6A, biuret and ammonium carbamate both have $\nu$(CO) greater than 1700 $cm^{-1}$, which makes them potential candidates to explain the unexpected IR absorption feature at 1731 $cm^{-1}$ when urea adsorbs on gold. However, upon adsorption, neither biuret nor ammonium carbamate give rise to a peak at 1731 $cm^{-1}$. Instead, peaks appear at 1660

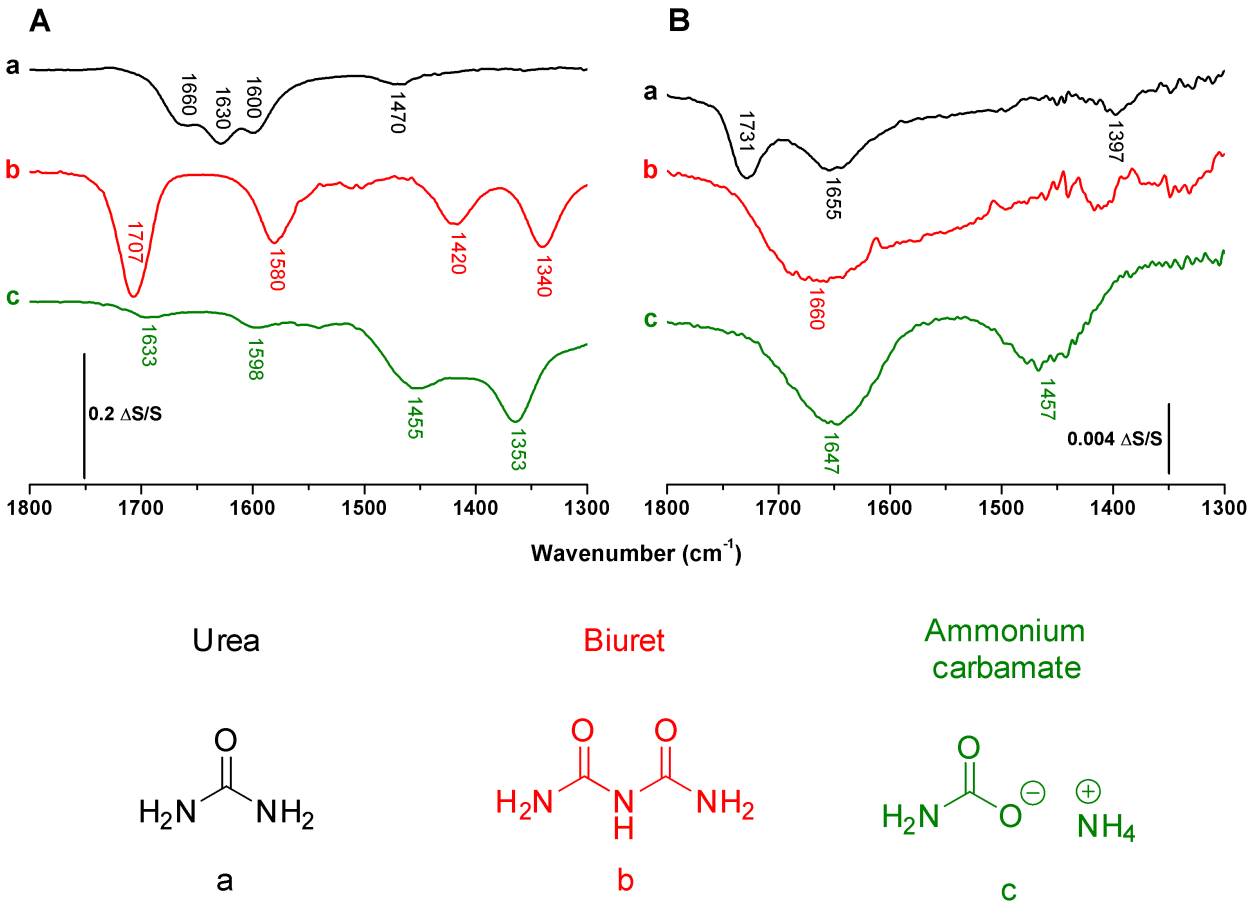


**Figure 4.6:** Transmission (A) and adsorption (B) spectra of urea and some of its potential breakdown products. (a): Urea (ATR), black (b): Biuret, red (c): Ammonium carbamate, green.

$cm^{-1}$ for biuret and 1647 and 1457 $cm^{-1}$ for ammonium carbamate, respectively. Ammonium carbamate is unstable and dissociates into $NH_3$ and $CO_2$ [164].

Cyanate exists in two resonance structures, one with a CO single bond and the other with a CO double bond. Therefore, its adsorption properties on gold were investigated even though no peaks appear around the carbonyl stretching region in transmission mode, instead a single very strong, peak appears at 2170 $cm^{-1}$, Figure 4.7A. Remarkably, cyanate provides a strong peak upon adsorption, Figure 4.7A, at 1734 $cm^{-1}$ even though this peak is not present in solution. Studies of cyanate adsorption have been performed on copper, platinum, rhodium, silver, and gold with no evidence of peaks in the carbonyl stretching region [165–171]. The study by Corrigan and Weaver includes a figure of the region between 2500 and 1000 $cm^{-1}$ which includes a weak peak at *ca* 1670 $cm^{-1}$ from -0.2 to 0 V vs SCE not attributed to cyanate. In the literature, the study of cyanate adsorption on gold produces multiple peaks [171] from 2168 to 2343 $cm^{-1}$, and 2102 to 2199 $cm^{-1}$ [168] from both adsorbed and solution phase species. In general, a peak from adsorbed cyanate is observed at $\sim$2200 $cm^{-1}$ for the $\nu$CN of N-bound cyanate. A peak at $\sim$2100 is attributed to adsorbed cyanide [168]. Experimentally, a single, very weak peak is observed at 2120 $cm^{-1}$ for the adsorption spectrum of urea on gold, Figure 4.7B. The absence of peaks in the expected cyanate adsorption region around 2200 $cm^{-}$ and the presence of two unexpected peaks at 1734 and 1621 $cm^{-1}$ in the carbonyl region indicate that cyanate, $OCN^{-}$, is not adsorbing to the surface. The presence of unexpected peaks suggests it undergoes a spontaneous reaction at the gold surface to form products with new vibrational peaks at 1734 and 1621 $cm^{-1}$, Figure 4.7A. Both peaks appear in the region for carbonyl stretches.

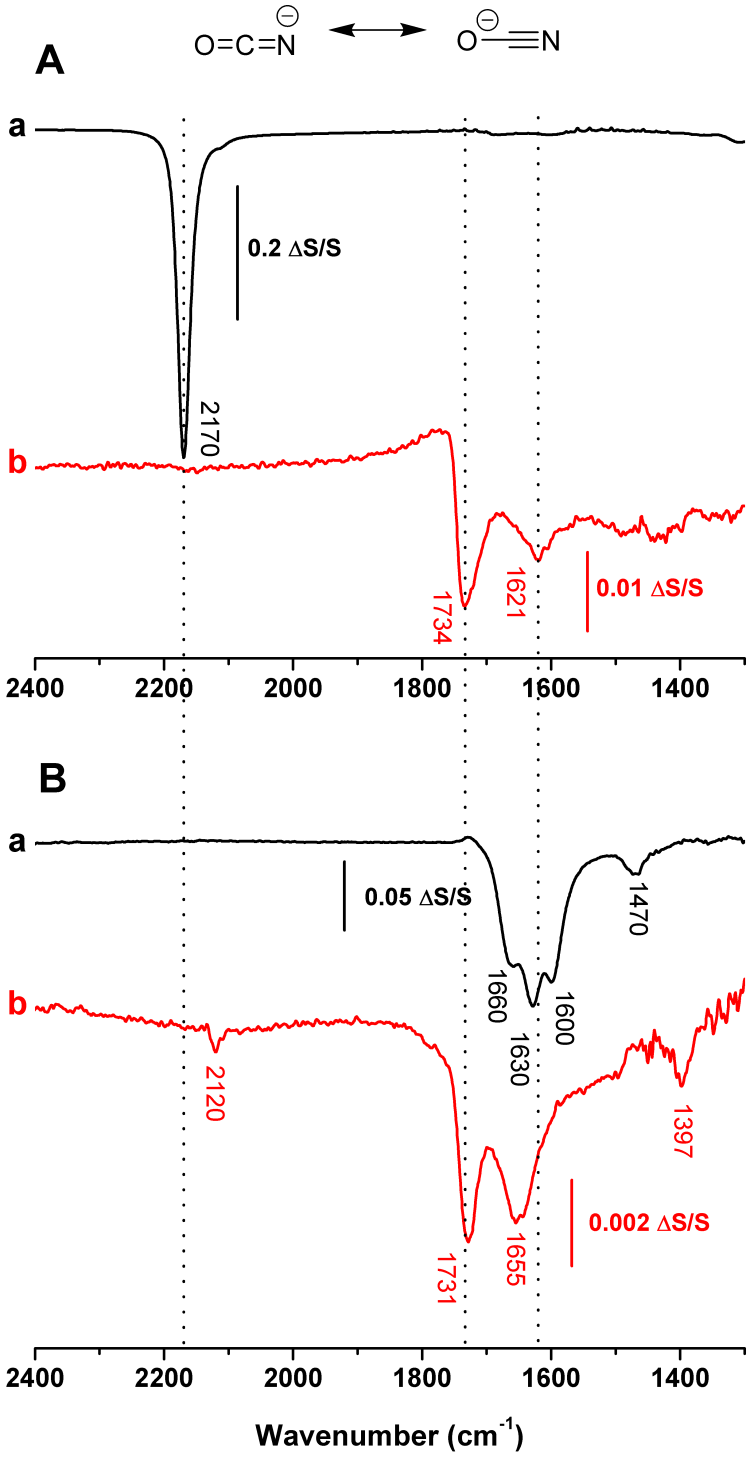


**Figure 4.7:** Transmission and adsorption spectra of Cyanate (A) and Urea (B) from 2400–1300 $cm^{-1}$. (a): Transmission, black (b) Adsorption, red.

The peak at 1734 $cm^{-1}$ matches that of adsorbed urea from Figure 4.7B, and as cyanate and urea exist in equilibrium [42] the peak likely results from formation of bidentate urea upon cyanate adsorption on gold (*vide infra*). Cumulatively, analysis of the possible breakdown products of urea upon adsorption on gold eliminates decomposition as the source of the unexpected peak at 1731 cm $^{-1}$.

The peak at 1731 $cm^{-1}$ likely results from another adsorption configuration of urea where the $\nu$(CO) is red-shifted to much higher wavenumbers. When urea adsorbs through both nitrogen atoms (**mode I**), the shift to high wavenumbers occurs as a result of reinforcement of the double bond character of CO. Adsorption through the second nitrogen subsequently weakens the CN bond. These results indicate urea adsorbs in two different configurations, **mode I** and **mode II**, possibly due to differences in adsorption on different crystal faces and the three peaks seen for urea adsorption on polycrystalline gold at the open circuit potential (OCP) are assigned as follows: 1731 $cm^{-1}$; $\nu$(CO,**I**), 1655 $cm^{-1}$; $\nu$(CO,**mode II**), and 1397; $\nu_{as}$(CN,**mode II**).

Possible interference from the water peak at 1650 $cm^{-1}$ leads to some ambiguity about these assignments as the peak for $\nu$(CO) of **mode II** is at a nearly identical wavenumber (1655 $cm^{-1}$). To better resolve the different urea adsorption modes and the assignment of the $\nu$(CO) modes, the experiment was repeated in $D_2O$. Upon deuteration, the water peak shifts to 1207 $cm^{-1}$, below the Si window cutoff, but introduces the potential of an HOD peak at 1432 $cm^{-1}$ [156]. In $D_2O$ (Figure 4.8B) four peaks are observed at 1706, 1595, 1549 and 1432 $cm^{-1}$ when urea adsorbs on gold. Comparing the $\nu$(CO) and $\nu_{as}$(CN) of adsorption to free urea in $D_2O$ (Figure 4.8A) there is a shift to 1595 and 1549 $cm^{-1}$ from 1606 and 1495 $cm^{-1}$, respectively. A small shift to lower wavenumbers for $\nu$(CO) and a shift to higher wavenumbers

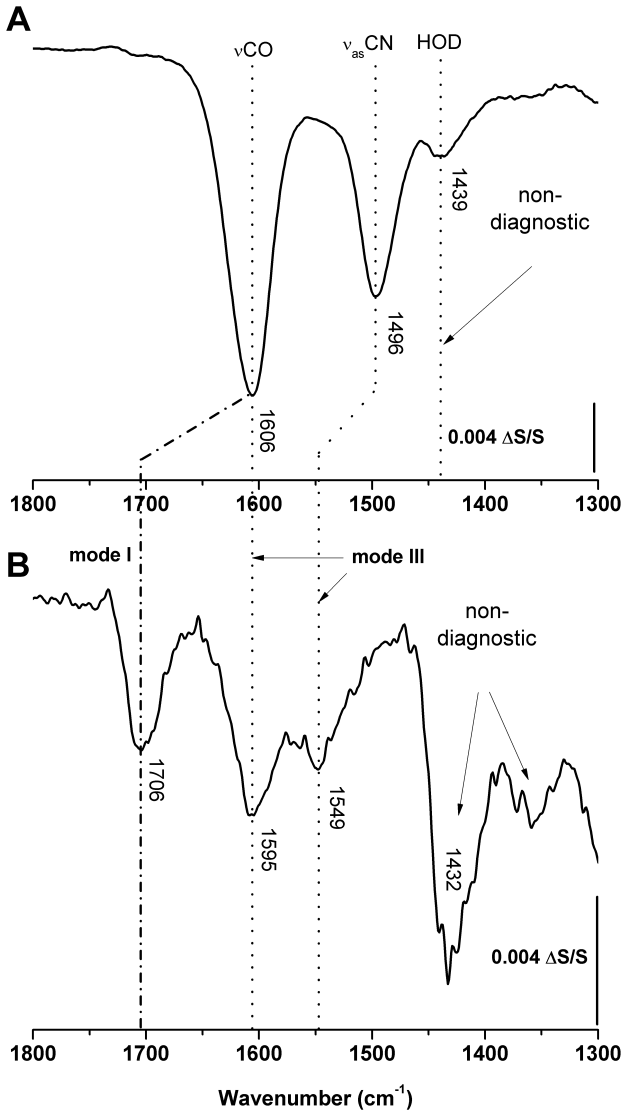


**Figure 4.8:** A) ATR spectra of urea and B) ATR SEIRAS spectra of urea adsorption on gold. In $D_2O$ based electrolyte.

for $\nu_{as}$(CN) indicate O-bonded urea that is tilted with respect to the metal surface, **mode III**. The presence of a peak at higher wavenumbers, 1706 $cm^{-1}$, and the absence of a second, corresponding $\nu_{as}$(CN) indicates urea is adsorbing through both nitrogen atoms (**mode I**). The peak at 1432 $cm^{-1}$ is an artifact caused by the drop in intensity of the single beam spectrum of urea below 1550 $cm^{-1}$.

In both the $H_2O$ and $D_2O$ experiments urea is adsorbed through two nitrogen atoms. In each case there is a second adsorption configuration. The $H_2O$ experiment exhibits **mode II** and the $D_2O$ experiment exhibits **mode III**. Two potential reasons for the different adsorptions are differences between individual gold layers which produce surfaces with crystal orientations that favor different orientation of the urea molecule, and changes in hydrogen bonding brought on by deuteration of the solvent and urea. Reproducible results indicate that the differences are not due to changes in surface morphology between individual gold layers therefore deuteration plays a non-neutral role in the spectral shift.

## 4.5 Behavior of urea adsorbed on gold thin films with applied potential

The adsorption configuration of a molecule can change with potential. Combining potential control with a spectroscopic technique like infrared spectroscopy provides information on processes, Faradaic or non-Faradaic, occurring at different potentials. Figure 4.9 shows the effect of changing the potential on the adsorption behavior of urea. Figure 4.9A shows urea adsorbed on gold before any potential is applied, Figure 4.9B shows its behavior as a function of potential during the first forward half of the sweep (oxidation) and Figure 4.9C

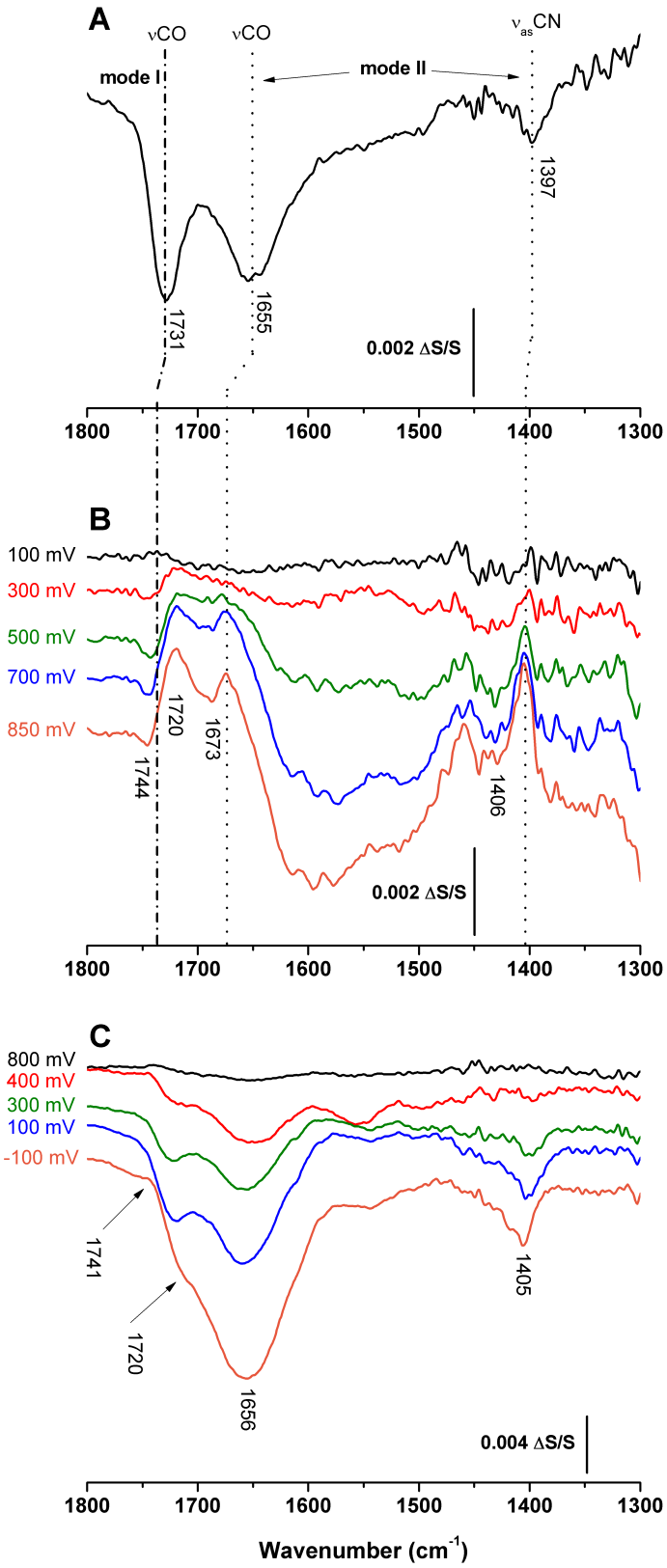


**Figure 4.9:** SEIRAS of 10 mM urea in 50 mM NaF in $H_2O$. A) At OCP (no applied potential, Ref: 50 mM NaF in $H_2O$); B) Forward half of the scan (Ref: Spectrum at OCP); C) Reverse half of the scan (Ref: Spectrum at 850 mV).

shows its behavior on the return portion of the sweep (reduction). After applied potential, urea returns to its original conformation with no applied potential (not shown) indicating the surface returns to its original configuration upon reduction of the remaining surface oxide.

In Figure 4.9B spectra are recorded at potentials from the OCP, ∼100 mV (black) to 850 mV (orange). Each spectrum is referenced to urea adsorbed on gold at the OCP (Figure 4.9A). The loss of two peaks associated with **mode II** at 1673 and 1406 $cm^{-1}$, starting at 500 mV, occur with increasing positive potential therefore urea is no longer adsorbed in this configuration, beyond 500 mV. The 1720 $cm^{-1}$ peak shifts to higher wavenumbers as a function of potential to form a bimodal peak centered around 1733 $cm^{-1}$ and is due to either a change in coverage or a vibrational Stark effect (shift to higher wavenumbers as a function of potential). SEIRAS spectra are essentially difference spectra. If a peak is present in the reference single beam spectrum but absent in the sample single beam spectrum it will result in an upward peak in the difference spectrum. If the negative feature shifts as a function of potential the resulting difference spectrum will exhibit bimodality. Similar results have been observed in previous work by this group [172]. Figure 4.10 shows the behavior of the 1720 $cm^{-1}$ peak as a function of potential (A) and a representative model of red shift that leads to this peak shape (B). In Figure 4.10B the black line represents the single-beam spectrum at the more negative potential, lower wavenumber, higher intensity peak while the red line represents the higher positive potential, higher wavenumber, lower intensity peak which, when taking the difference spectra, leads to the blue peak shape. The peak maxima and minima are shifted after the subtraction and normalization. If both peaks were the same magnitude the higher wavenumber (downward) part of the bimodal peak at 1745 $cm^{-1}$ would be much more intense. The shape of the bimodal peak indicates a decrease in intensity

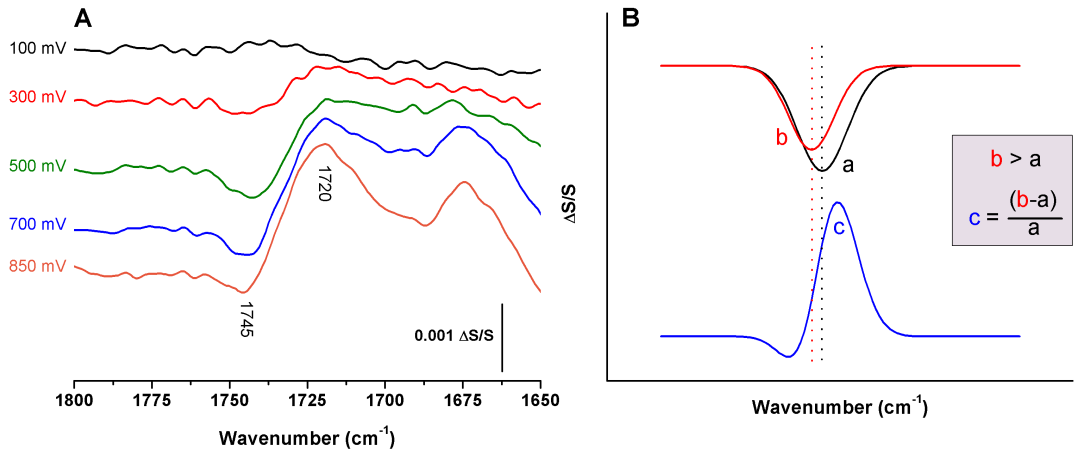


**Figure 4.10:** Behavior of the peak at 1720 $cm^{-1}$ as a function of potential from Figure 4.9B. Red (b) and Black (a): peak models at more negative (black) and more positive (red) potentials. Blue (c): Difference spectra of black and red.

with increasing potential therefore some **mode I** must be desorbing. The decrease in peak intensity coincides with the onset of gold oxidation therefore urea must not adsorb on gold oxide.

Figure 4.9C shows the adsorption of urea on gold during the return sweep, starting at 850 mV (the reference potential) and taking spectra at various potentials from 800 mV (black line) to -100 mV (orange line). A peak at 1405 $cm^{-1}$ ($\nu_{as}$(CN) of adsorbed urea) appears at 300 mV and increases in intensity with less positive potential. The urea appears to readsorb in the **mode II** configuration at low positive potentials. The $\nu$(CO) peak of adsorbed urea overlaps the OH stretch of $H_2O$ at 1656 $cm^{-1}$. At potentials below 800 mV two small peaks appear at 1741 and 1720 $cm^{-1}$ (downward). The peaks are opposite from the forward scan as in the $\nu$(CO) peak shifts to lower wavenumbers due to the more positive applied potential.

The electrochemical experiment was repeated in $D_2O$ and the results are shown in Figure 4.11. Figure 4.11A shows urea adsorption on gold with no applied potential and is the reference for Figure 4.11B. Upon applying increasingly positive potentials (Figure 4.11B)

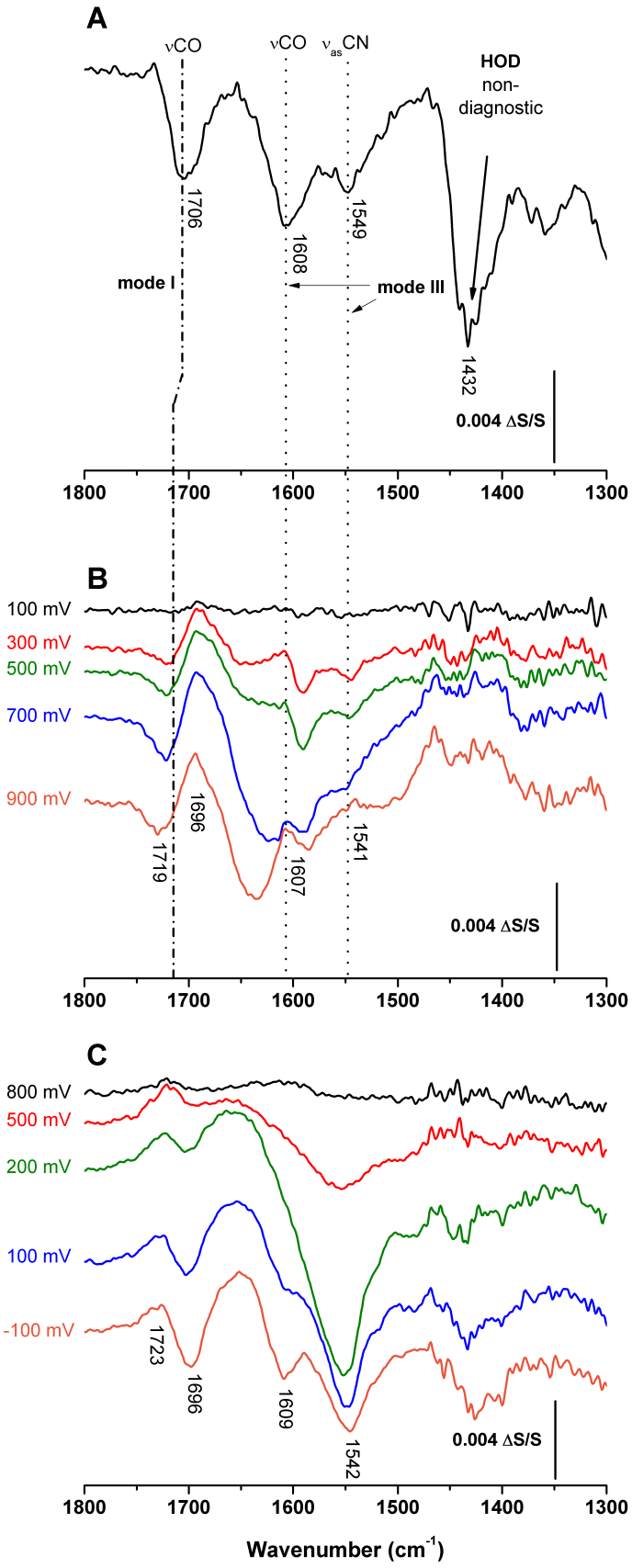


**Figure 4.11:** SEIRAS of 10 mM urea in 50 mM NaF in $D_2O$. A) At OCP (no applied potential, Ref: 50 mM NaF in $D_2O$); B) Forward half of the scan (Ref: Spectrum at OCP); C) Reverse half of the scan (Ref: Spectrum at 900 mV).

the two peaks at 1608 and 1549 $cm^{-1}$ associated with adsorption through the oxygen atom, **mode III**, increase in intensity until 400 mV and remain constant up until 700 mV where the peak at 1549 $cm^{-1}$ disappears and the peak at 1595 $cm^{-1}$ is diminished but remains very weak which indicates the incomplete loss of **mode III**. The **mode I** species is still present and its $\nu$(CO) peak at 1706 $cm^{-1}$ shifts to higher wavenumbers as a function of increasing potential forming a bimodal peak centered on 1709 $cm^{-1}$ and does not desorb.

In Figure 4.11C the potential is reversed to -100 mV from 800. The $\nu$(CO) and $\nu_{as}$(CN) peaks for **mode III** at 1609 and 1542 $cm^{-1}$ reappear at 100 and 500 mV, respectively. The 1609 $cm^{-1}$ peak returns to its original intensity at -100 mV but the latter increases rapidly in intensity, reaching a maximum at 200 mV, then decreases and remains constant after 0 mV which means it has reached maximum coverage. The appearance of an $\nu_{as}$(CN) without the corresponding $\nu$(CO), observed from 100–500 mV, was also observed for **mode III** on Rh(111) and is attributed to urea adsorbed with a high degree of tilting resulting in a transition dipole moment for $\nu$(CO) parallel with the metal surface [9]. The high wavenumber $\nu$(CO) peak associated with **mode I** blue shifts as a function of potential. Figure 4.12 shows the behavior of the 1706 $cm^{-1}$ peak as a function of potential (A) and a representative model of the blue shift that leads to this peak shape (B). In Figure 4.12B, at the more positive potential the peak is at a higher wavenumber with a lower intensity while at the less negative potential is a lower wavenumber, higher intensity peak which, when taking the difference spectra, leads to the blue peak shape. The intensity of the peak increases as the potential is made more positive, indicating the **mode I** species is readsorbing.

In summary, urea adsorption on gold occurs through multiple configurations. In $H_2O$ urea adsorbs through a single nitrogen atom with peaks at 1655 and 1397 $cm^{-1}$ and through

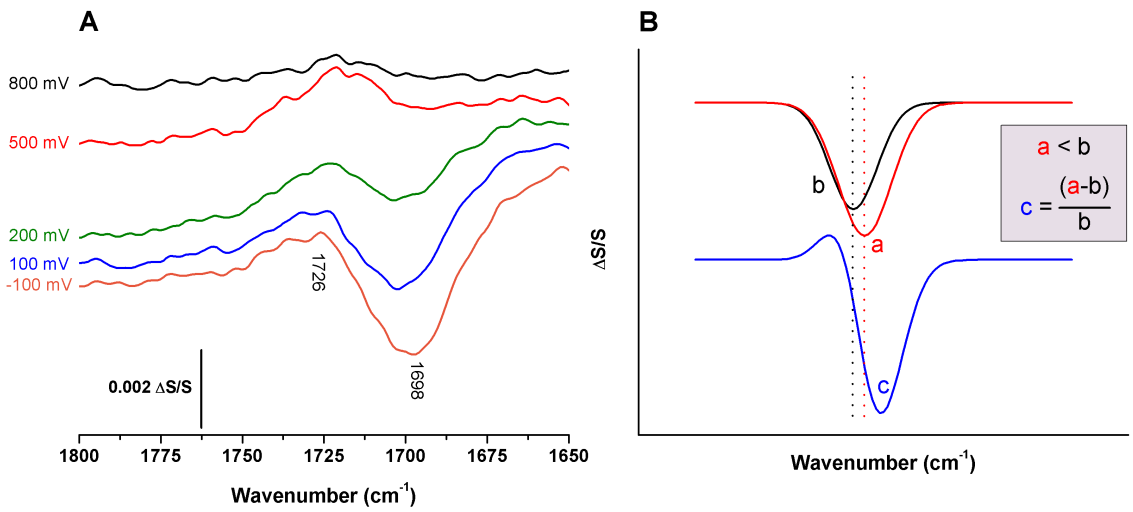


**Figure 4.12:** Behavior of the peak at 1706 $cm^{-1}$ as a function of potential from Figure 4.11B. Red (a) and Black (b): peak models at more positive (black) and more negative (red) potentials. Blue (c): Difference spectra of black and red.

both nitrogens with a peak at 1721 $cm^{-1}$. At potentials more positive than the OCP, **mode I** partially desorbs and shifts to a higher wavenumbers, resulting in a bimodal peak in the range of 1744–1720 $cm^{-1}$. Upward going peaks appear at 1673 and 1406 $cm^{-1}$ and indicate a loss of the **mode II** species. Upon return to more negative potentials, it appears that **mode II** readsorbs due to the return of the 1406 $cm^{-1}$ peak. The **mode I** species shifts to lower wavenumbers. Interpretation is made ambiguous by $\nu$(CO) and water having peaks at similar wavenumbers.

Urea adsorption on gold in $D_2O$ is similar. Adsorption occurs through two nitrogen atoms as is indicated by the peak at 1706 $cm^{-1}$. Peaks at 1608 and 1549 $cm^{-1}$ indicate **mode III** tilted with respect to the surface. A peak at 1432 $cm^{-1}$ results from an artifact. At more positive potentials **mode I** desorbs partially and shifts to higher wavenumbers as a function of potential, resulting in a bimodal peak in the range of 1719–1696 $cm^{-1}$. Upward going peaks appear at 1607 and 1541 $cm^{-1}$ and indicate a loss of the **mode III** species. Upon

return to more negative potentials, the **mode I** shifts to lower wavenumbers. Two peaks associated with **mode III**, 1609 and 1542 $cm^{-1}$, return at 100 and 500 mV respectively. When readsorption occurs urea has a a higher degree of tilting with respect to the surface at more positive potentials and becomes more normal as the potential is made more negative.

This is summarized in the following scheme:

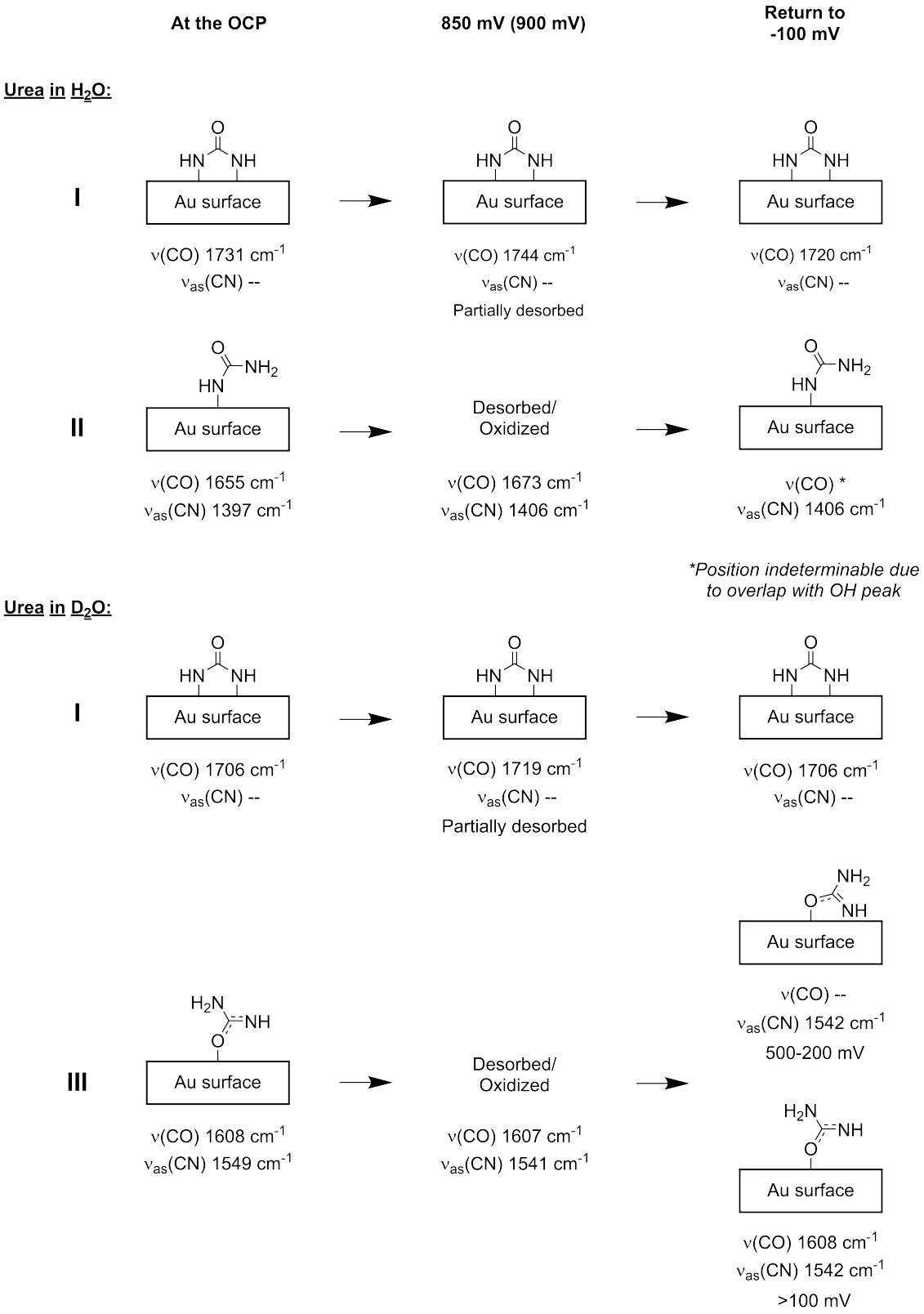


**Scheme 4.2:** Summary of the behavior of urea adsorption on Au in $H_2O$ and $D_2O$ experiments.

# Chapter 5

# Conclusions and Future Work

## 5.1 Conclusions

The adsorption configuration of urea on a polycrystalline gold surface was measured using a combination of electrochemical (CV and DC), spectroscopic (IR and ATR-IR), and spectro-electrochemical (SEIRAS) techniques. Measurements were performed in a neutral solution of sodium fluoride in both $H_2O$ and $D_2O$.

In a solution of $H_2O$, urea adsorbed in **mode I** and **mode II**. When the applied potential was more positive than the OCP, **mode II** desorbed while **mode I** shifted to higher wavenumbers, resulting in a bimodal peak, and partially desorbed. Upon return to more negative potentials, **mode I** readsorbed and **mode II** presumably readsorbed but interpretation was ambiguous due to interference from the solvent peak.

Urea adsorption on gold in $D_2O$ was found to be similar to that of $H_2O$. Urea adsorbed in **mode I** and **mode III**. When the applied potential was more positive than the OCP **mode III** desorbed and **mode I** shifted to higher wavenumbers and partially desorbed. Upon return to more negative potentials, both **mode I** and **mode III** readsorbed. **Mode III** was initially strongly tilted, resulting in $\nu$(CO) parallel to the surface and unobservable, but gradually the molecule became less tilted and the $\nu$(CO) reappeared.

Systematic elimination of breakdown products of urea oxidation confirmed that urea adsorption was the only process occurring at the gold surface from a solution containing urea. Upon investigation of the adsorption of cyanate, $OCN^-$, as a potential breakdown product of urea it was determined that it produced a peak at the same wavenumber as urea adsorbed through both nitrogen atoms, **mode I**, and must therefore be acting to reform urea on the gold surface. Ammonium carbamate and biuret were not formed and did not act to reform urea on contact with the gold surface.

Assignments of the adsorption modes of urea was done by comparing peaks in the SEIRAS spectra to those assigned on Pt(100), Pt(110) and Pt(111), and Rh(100), Rh(110) and Rh(111). In $H_2O$ and $D_2O$ experiments urea adsorbs through **mode I** and behaves similarly to urea on Pt(100) and Rh(100) by remaining adsorbed at all potentials. Therefore, assuming urea behaves similarly when adsorbed to Au(100) as to Pt(100) and Rh(100) it is likely that urea is adsorbed through both nitrogen atoms, **mode I**, on Au(100). In addition, previous FT-IR experiments on Au(100) have indicated that $\nu$(CO) is perpendicular to the gold surface [11]. However, confirmation of the conclusion necessitates experiments using an Au(100) electrode.

The adsorption behavior of the two other modes, **mode II** in $H_2O$ and **mode III** in $D_2O$ did not match the behavior of urea on platinum or rhodium. On gold, urea desorbed at high potentials while on platinum and rhodium it remained adsorbed and changed bonding mode. Urea adsorbed to gold did not change bonding mode with applied potential. Urea adsorption appeared to be stronger on platinum and rhodium than on gold when considering **mode II** and **mode III**. The adsorption of urea on gold in $D_2O$ resulted in a high degree of tilting which is similar to that observed of the adsorption of urea on Rh(111).

The use of noble metals for urea oxidation as a method of wastewater treatment, based on these results and those described in the literature, has limitations. Ideally, processes should occur with the requirement of as little energy input as possible. Logically, the treatment of waste-rich water using electro-oxidation would occur with a low applied potential, especially if none of the products of water treatment are being reclaimed for other purposes. The results that urea remains adsorbed to gold up to the most positive potential measured, 0.9 V vs Ag/AgCl, and oxidation of urea has not occurred is problematic. From CV data, the increase in current due to the oxidation of gold had just begun, indicating that at high positive potentials urea either does not adsorb on gold oxide and begins to desorb, is oxidized or a combination of both. The peak potential, 1.0 V vs Ag/AgCl, is a large potential to apply to drive the oxidation forward. On gold, **mode II** and **mode III** desorb while **mode I** remains adsorbed to the electrode surface. Assuming the desorption frees the surface to allow oxidation to occur or that the desorption is due to oxidation of the urea it can be concluded that an electrocatalyst would need a surface consisting of the faces to which urea is most weakly adsorbed. Creating these electrodes would be more difficult if these were high energy faces. Higher energy faces are likely not stable for the long period a successful catalyst would require.

Literature has hinted at the potential to convert urea-rich wastewater into a fuel source [54, 55] through the production of $H_2$. This requires a clean conversion of urea to products as described in Section 1.3. As none of these products can be measured using IR spectroscopy it is inconclusive whether that process is occurring on gold. Further experiments aimed at the measurement of these products could be performed using techniques specific to each product. Detection could be performed using a technique like mass spectrometry where the production

of ions of a specific mass to charge ratio can be monitored. DEMS has already been employed for this purpose using platinum for the oxidation of urea [13].

## 5.2 Future Work

The effect of solvent on the adsorption and electro-oxidation of urea is unexpected and interesting. The characterization of urea adsorption on gold indicated that the adsorption modes were different under different experimental conditions. In $H_2O$ urea adsorbed through **mode I** and **mode II** but in $D_2O$ urea adsorbed through **mode I** and **mode III**. There were two differences between the experiments: each was performed on a new gold layer and the solvent was $H_2O$ in one and $D_2O$ in the other. Differences in the gold layer were eliminated due to the reproducibility of results therefore isotopic substitution of hydrogen for deuterium plays a role in experimental differences in the adsorption of urea and is an interesting effect that merits further investigation.

The short term goal was to characterize the adsorption of urea on a polycrystalline gold surface using SEIRAS. Results from these experiments will be used as a reference for the long term goal of characterization of the adsorption of urea on a base metal surface deposited on the thin gold film.

Ultimately, the system that has been chosen to test SEIRAS on metals other than gold is the electro-oxidation of urea on a nickel electrode in basic solution. The use of a gold underlayer to perform surface enhanced experiments has been successfully demonstrated using nickel [149]. The investigation of the adsorption of CO and pyridine on Ni surfaces was performed using SEIRAS on a thin nickel film deposited on a thin gold film. It was

determined that adsorption of pyridine occurred through the nitrogen atom with a tilted configuration and that CO adsorbed to the surface without resulting in inverted or bipolar bands.

Formation of the required working electrode is a non-trivial process. The deposition of nickel onto a gold bead working electrode can be accomplished using a modified Watt's bath made of $H_3BO_3$, $NiSO_4$ and HCl using a potential of -1 V [173]. Huo *et al.* employed this method to create their nickel/gold layers. Modifications would need to be made to ensure the thin gold layers can withstand the harsh nickel deposition conditions. For example at an applied potential of -1 V vs Ag/AgCl there is significant hydrogen evolution, forming bubbles, which can lead to the destruction of the gold film.

Preliminary experiments have been performed to find milder conditions by lowering the deposition potential and depositing for a longer time period however optimized conditions have not been determined. Ideally, the nickel layer needs to be complete as to avoid interfering signals from the underlying gold layer but needs to remain thin enough to ensure penetration of the evanescent wave and maintain the surface enhancement effect. Alternatively, any holes where nickel has not deposited could be "covered up" using a molecule that strongly adsorbs to gold, and not nickel, and will remain adsorbed to gold through SEIRAS experiments. An ideal candidate would be a thiol such as octadecanethiol which does not adsorb to nickel oxide and forms ordered layers on gold and does not desorb until well below -1 V vs Ag/AgCl [174]. Some initial experiments have been performed and produced promising results.

The electro-oxidation of urea on Ni in basic conditions yields [63] $N_2$, $H_2O$ and $CO_2$ by Equation 5.1.

$$CO(NH_2)_2 + H_2O \rightarrow N_2 + 3H_2 + CO_2 \tag{5.1}$$

Two mechanisms have been proposed for the electro-oxidation of urea on nickel in basic media: a direct [54] and an indirect [63] mechanism. Both have the same cathode reaction (Equation 5.2) and the same overall reaction (Equation 5.1) but different reactions at the anode. The direct mechanism occurs through reactions 5.3 and 5.4, where in the first step the $NiOOH_{(s)}$ formed at potentials above 0.47 V vs Ag/AgCl provides the $OH^-$ necessary to catalyze the oxidation of urea, Equation 5.4.

$$6H_2O_{(l)} + 6e^- \rightarrow 3H_{2(g)} + 6OH^-_{(aq)} \tag{5.2}$$

$$Ni(OH)_{2(s)} + OH^-_{(aq)} \rightleftharpoons NiOOH_{(s)} + H_2O_{(l)} + e^- \tag{5.3}$$

$$CO(NH_2)_{2(aq)} + 6OH^-_{(aq)} \rightarrow 5H_2O_{(l)} + N_{2(g)} + CO_{2(g)} + 6e^- \tag{5.4}$$

In the indirect mechanism the first step of the reaction is the same as Equation 5.3 but the $NiOOH_{(s)}$ formed reacts in a chemical reaction to form the products as in Equation 5.5.

$$6NiOOH_{(s)} + CO(NH_2)_{2(aq)} + H_2O_{(aq)} \rightarrow 6Ni(OH)_{2(s)} + N_{2(g)} + CO_{2(g)} \tag{5.5}$$

Addition of Equation 5.5 and Equation 5.3 gives the same overall equation as the direct mechanism. The use of SEIRAS on nickel films will help to elucidate the mechanism for

this reaction by measuring changes of the nickel film as the reaction is occurring. First steps include measuring changes in the nickel layer as a function of potential in basic media. The results will be used to establish a reference for spectral changes occurring due to changes in the nickel surface. The comparison of results on Ni with and without urea can be used to determine the effect of the electro-oxidation of urea on the nickel surface. For this reason it will be interesting to compare urea adsorption on nickel and gold due to the differences in their electrochemical behavior.

# Bibliography


[1] Raunier,; Raunier, S.; Chiavassa, T.; Duvernay, F.; Borget, F.; Aycard, J. P.; Dartois, E.; d'Hendecourt, L. *Astronomy & Astrophysics* **2004**, *416*, 5.

[2] Rouelle, M. *Journal de médecine, chirurgie, pharmacie* **1773**, *40*, 451–468.

[3] Tsipis, C. A.; Karipidis, P. A. *J. Am. Chem. Soc.* **2003**, *125*, 2307–2318.

[4] Wöhler, F. *Ann. Phys.* **1828**, *88*, 253–256.

[5] Theophanides, T.; Harvey, P. D. *Coordination Chemistry Reviews* **1987**, *76*, 237–264.

[6] Climent, V.; Rodes, A.; Orts, J. M.; Feliu, J. M.; Pérez, J. M.; Aldaz, A. *Langmuir* **1997**, *13*, 2380–2389.

[7] Climent, V.; Gòmez, R.; Herrero, E.; Orts, J. M.; Rodes, A.; Feliu, J. M. *Colloids and Surfaces A: Physicochemical and Engineering Aspects* **1998**, *134*, 133–143.

[8] Climent, V.; Rodes, A.; Orts, J. M.; Aldaz, A.; Feliu, J. M. *Journal of Electroanalytical Chemistry* **1999**, *461*, 65–75.

[9] Climent, V.; Rodes, A.; Pérez, J. M.; Feliu, J. M.; Aldaz, A. *Langmuir* **2000**, *16*, 10376–10384.

[10] Climent, V.; Rodes, A.; Albalat, R.; Claret, J.; Feliu, J. M.; Aldaz, A. *Langmuir* **2001**, *17*, 8260–8269.

[11] Nakamura, M.; Song, M. B.; Ito, M. *Surface Science* **1999**, *427-428*, 167–172.

[12] Bezerra, A. C. S.; de Sá, E. L.; Nart, F. C. *J. Phys. Chem. B* **1997**, *101*, 6443–6449.

[13] Bolzan, A. E.; Iwasita, T. *Electrochimica Acta* **1988**, *33*, 109–112.

[14] Rikvold, P. A.; Wieckowski, A. *Phys. Scr.* **1992**, *1992*, 71.

[15] Rubel, M.; Rhee, C. K.; Wieckowski, A.; Rikvold, P. A. *Journal of Electroanalytical Chemistry and Interfacial Electrochemistry* **1991**, *315*, 301–306.

[16] Rhee, C. K. *Journal of the Electrochemical Society* **1992**, *139*, 13C–19C.

[17] Van Alsenoy, C.; Williams, J. O.; Schäfer, L. *Journal of Molecular Structure: THEOCHEM* **1981**, *76*, 179–185.

[18] Koizumi, M.; Tachibana, A.; Yamabe, T. *Journal of Molecular Structure: THEOCHEM* **1988**, *164*, 37–47.

[19] Williams, M. L.; Gready, J. E. *J. Comput. Chem.* **1989**, *10*, 35–54.

[20] Vijay, A.; Sathyanarayana, D. N. *Journal of Molecular Structure* **1993**, *295*, 245–258.

[21] Meiers, R. J.; Coussens, B. *Journal of Molecular Structure: THEOCHEM* **1992**, *253*, 25–33.

[22] Ramondo, F.; Bencivenni, L.; Rossi, V.; Caminiti, R. *Journal of Molecular Structure: THEOCHEM* **1992**, *96*, 185–211.

[23] Gobbi, A.; Frenking, G. *J. Am. Chem. Soc.* **1993**, *115*, 2362–2372.

[24] Ha, T.-K.; Puebla, C. *Chemical Physics* **1994**, *181*, 47–55.

[25] Kellner, L. *Proceedings of the Royal Society of London A: Mathematical, Physical and Engineering Sciences* **1941**, *177*, 456–475.

[26] Keuleers, R.; Desseyn, H. O.; Rousseau, B.; Van Alsenoy, C. *J. Phys. Chem. A* **1999**, *103*, 4621–4630.

[27] Hadži, D.; Kidrič, J.; Kneževic, Z. V.; Barlič, B. *Spectrochimica acta. Part A, Molecular and biomolecular spectroscopy* **1976**, *32no*, 693–704.

[28] Rajalakshmi, T.; Fareed, R. S. Q.; Dhanasekaran, R.; Ramasamy, P.; Thomas, J.; Srinivasan, K. *Materials Science and Engineering: B* **1996**, *39*, 111–115.

[29] Yamaguchi, A.; Miyazawa, T.; Shimanouchi, T.; Mizushima, S. *Spectrochimica Acta* **1957**, *10*, 170–178.

[30] Díaz, G.; Campos, M. *Spectroscopy Letters* **1981**, *14*, 365–377.

[31] Derreumaux, P.; Vergoten, G.; Lagant, P. *J. Comput. Chem.* **1990**, *11*, 560–568.

[32] Saito, Y.; Machida, K.; Uno, T. *Spectrochimica Acta Part A: Molecular Spectroscopy* **1971**, *27*, 991–1002.

[33] García-Hernández, M.; Birkenheuer, U.; Hu, A.; Illas, F.; Rösch, N. *Surface Science* **2001**, *471*, 151–162.

[34] Brandts, J. F.; Hunt, L. *J. Am. Chem. Soc.* **1967**, *89*, 4826–4838.

[35] Watlaufer, D. B.; Malik, S. K.; Stoller, L.; Coffin, R. L. *J. Am. Chem. Soc.* **1964**, *86*, 508–514.

[36] Schick, M. J. *J. Phys. Chem.* **1964**, *68*, 3585–3592.

[37] Andrew, E. R.; Hyndman, D. *Discuss. Faraday Soc.* **1955**, *19*, 195–200.

[38] Holze, R.; Schomaker, S. *Electrochimica Acta* **1990**, *35*, 613–620.

[39] Wang, D.; Botte, G. G. *ECS Electrochem. Lett.* **2014**, *3*, H29–H32.

[40] Meessen, J. H. *Ullmann's Encyclopedia of Industrial Chemistry*; Wiley-VCH Verlag GmbH & Co. KGaA, 2000.

[41] Shaw, W. H. R.; Bordeaux, J. J. *J. Am. Chem. Soc.* **1955**, *77*, 4729–4733.

[42] Dirnhuber, P.; Schütz, F. *Biochem J* **1948**, *42*, 628–632.

[43] Belson, D. J.; Strachan, A. N. *Chem. Soc. Rev.* **1982**, *11*, 41–56.

[44] Kaasenbrood, P. J. C.; Van Den Berg, P. J.; Revallier, L. J. *J. Agric. Food Chem.* **1963**, *11*, 39–43.

[45] Ostrogovich, G.; Bacaloglu, R. *Revue Roumaine de Chimie* **1965**, *10*, 1111–1123.

[46] Brack, W.; Heine, B.; Birkhold, F.; Kruse, M.; Schoch, G.; Tischer, S.; Deutschmann, O. *Chemical Engineering Science* **2014**, *106*, 1–8.

[47] Epperly, R. *CHEMTECH* **1991**, *21*, 429–431.

[48] Rudman, D.; DiFulco, T. J.; Galambos, J. T.; Smith, R. B.; Salam, A. A.; Warren, W. D. *J Clin Invest* **1973**, *52*, 2241–2249.

[49] Häussinger, D. *The Textbook of Hepatology: From Basic Science to Clinical Practice*, 3rd ed.; Wiley-Blackwell, 2007; pp 181–192.

[50] Rahimpour, M. R. *Chemical Engineering and Processing: Process Intensification* **2004**, *43*, 1299–1307.

[51] Hüttl, R.; Bohmhammel, K.; Wolf, G.; Oehmgen, R. *Thermochimica Acta* **1995**, *250*, 1–12.

[52] Zaborska, W.; Leszko, M. *Polish Journal of Chemistry* **1994**, *68*, 2733–2739.

[53] Gupta, S. K.; Sharma, R. *Water Research* **1996**, *30*, 593–600.

[54] Boggs, B.; L. King, R.; G. Botte, G. *Chemical Communications* **2009**, *0*, 4859–4861.

[55] King, R. L.; Botte, G. G. *Journal of Power Sources* **2011**, *196*, 2773–2778.

[56] Ji, R.-Y.; Chan, D.-S.; Jow, J.-J.; Wu, M.-S. *Electrochemistry Communications* **2013**, *29*, 21–24.

[57] Liang, Y.; Liu, Q.; Asiri, A. M.; Sun, X. *Electrochimica Acta* **2015**, *153*, 456–460.

[58] Miller, A.; Hassler, B.; Botte, G. *Journal of Applied Electrochemistry* **2012**, *42*, 925–934.

[59] Wang, D.; Yan, W.; Botte, G. G. *Electrochemistry Communications* **2011**, *13*, 1135–1138.

[60] Wang, D.; Yan, W.; Vijapur, S. H.; Botte, G. G. *Electrochimica Acta* **2013**, *89*, 732–736.

[61] Wu, M.-S.; Lin, G.-W.; Yang, R.-S. *Journal of Power Sources* **2014**, *272*, 711–718.

[62] Daramola, D. A.; Singh, D.; Botte, G. G. *J. Phys. Chem. A* **2010**, *114*, 11513–11521.

[63] Vedharathinam, V.; Botte, G. G. *Electrochimica Acta* **2012**, *81*, 292–300.

[64] Yan, W.; Wang, D.; Botte, G. G. *Applied Catalysis B: Environmental* **2012**, *127*, 221–226.

[65] Vedharathinam, V.; Botte, G. G. *Electrochimica Acta* **2013**, *108*, 660–665.

[66] Quirk, A.; Unni, B.; Burgess, I. J. *Langmuir* **2016**, *32*, 2184–2191.

[67] Quirk, A.; Lardner, M. J.; Tun, Z.; Burgess, I. J. *Langmuir* **2016**, *32*, 2225–2235.

[68] Werner, E. A. *J. Chem. Soc., Trans.* **1912**, *101*, 2166–2180.

[69] Hynd, A.; Macfarlane, M. G. *Biochem J* **1926**, *20*, 1264–1272.

[70] Hunter, E. C. E.; Partington, J. R. *J. Chem. Soc.* **1933**, 87–90.

[71] Devoto, G. *Gazzetta Chimica Italiana* **1933**, *63*, 119–121.

[72] Bergmann, E.; Weizmann, A. *Trans. Faraday Soc.* **1938**, *34*, 783–786.

[73] Pauling, L.; Brockway, L. O.; Beach, J. Y. *J. Am. Chem. Soc.* **1935**, *57*, 2705–2709.

[74] Wyckoff, R. W. G. *Zeitschrift für Kristallographie - Crystalline Materials* **1932**, *81*, 102–109.

[75] Wyckoff, R. W. G.; Corey, R. B. *Zeitschrift für Kristallographie - Crystalline Materials* **1934**, *89*, 462–468.

[76] Vaughan, P.; Donohue, J. *Acta Cryst.* **1952**, *5*, 530–535.

[77] Sklar, N.; Senko, M. E.; Post, B. *Acta Cryst.* **1961**, *14*, 716–720.

[78] Caron, A.; Donohue, J. *Acta Cryst.* **1964**, *17*, 544–546.

[79] Caron, A.; Donohue, J. *Acta Cryst. B* **1969**, *25*, 404–404.

[80] Swaminathan, S.; Craven, B. M.; Spackman, M. A.; Stewart, R. F. *Acta Cryst. B* **1984**, *40*, 398–404.

[81] Worsham, J. E.; Levy, H. A.; Peterson, S. W. *Acta Cryst.* **1957**, *10*, 319–323.

[82] Pryor, A. W.; Sanger, P. L. *Acta Cryst. A* **1970**, *26*, 543–558.

[83] Guth, H.; Heger, G.; Klein, S.; Treutmann, W.; Scheringer, C. *Zeitschrift für Kristallographie* **1980**, *153*, 237–254.

[84] Godfrey, P. D.; Brown, R. D.; Hunter, A. N. *Journal of Molecular Structure* **1997**, *413-414*, 405–414.

[85] King, S. T. *Spectrochimica Acta Part A: Molecular Spectroscopy* **1972**, *28*, 165–175.

[86] Brown, R. D.; Godfrey, P. D.; Storey, J. *Journal of Molecular Spectroscopy* **1975**, *58*, 445–450.

[87] Li, X.; Stotesbury, S. J.; Jayasooriya, U. A. *Spectrochimica Acta Part A: Molecular Spectroscopy* **1987**, *43*, 1595–1597.

[88] Cirino, J. J. V.; Bertran, C. A. *Química Nova* **2002**, *25*, 358–363.

[89] Inostroza, N.; Senent, M. L. *Chemical Physics Letters* **2012**, *524*, 25–31.

[90] Angus, W.; Bailey, C.; Hale, J.; Ingold, C.; Leckie, A.; Raisin, C.; Thompson, J.; Wilson, C. *Journal of the Chemical Society* **1936**, 971–987.

[91] Sutherland, G. B. B. M.; Dennison, D. M. *Proceedings of the Royal Society of London A: Mathematical, Physical and Engineering Sciences* **1935**, *148*, 250–271.

[92] Kohlrausch, K. *Physikalische Zeitschrift* **1931**, *32*, 385–406.

[93] Dixon, D. A.; Matsuzawa, N. *J. Phys. Chem.* **1994**, *98*, 3967–3977.

[94] Spoliti, M.; Pieretti, A.; Bencivenni, L.; Sanna, N. *Electron. J. Theor. Chem.* **1997**, *2*, 149–159.

[95] Laulicht, I.; Pinchas, S.; Petreanu, E.; Samuel, D. *Spectrochimica Acta* **1965**, *21*, 1487–1494.

[96] Stewart, J. E. *The Journal of Chemical Physics* **1957**, *26*, 248–254.

[97] Duncan, J. L. *Spectrochimica Acta Part A: Molecular Spectroscopy* **1971**, *27*, 1197–1205.

[98] Arenas, J.; Parellada, R. *Journal of Molecular Structure* **1971**, *10*, 253–264.

[99] Robinson, T. S.; Price, W. C. *Proc. Phys. Soc. B* **1953**, *66*, 969.

[100] Liapis, K.; Jayasooriya, U. A.; Kettle, S. F. A.; Eckert, J.; Goldstone, J. A.; Taylor, A. D. *J. Phys. Chem.* **1985**, *89*, 4560–4565.

[101] Durman, R.; Jayasooriya, U. A.; Kettle, S. F. A. *J. Phys. Chem.* **1988**, *92*, 620–622.

[102] Gamboa-Aldeco, M.; Mrozek, P.; Rhee, C. K.; Wieckowski, A.; Rikvold, P. A.; Wang, Q. *Surface Science* **1993**, *297*, L135–L140.

[103] Rikvold, P. A.; Gamboa-Aldeco, M.; Zhang, J.; Han, M.; Wang, Q.; Richards, H. L.; Wieckowski, A. *Surface Science* **1995**, *335*, 389–400.

[104] Rikvold, P. A.; Zhang, J.; Sung, Y. E.; Wieckowski, A. *Electrochimica Acta* **1996**, *41*, 2175–2184.

[105] Alexandrova, A. N.; Jorgensen, W. L. *J. Phys. Chem. B* **2007**, *111*, 720–730.

[106] Callahan, B. P.; Yuan, Y.; Wolfenden, R. *J. Am. Chem. Soc.* **2005**, *127*, 10828–10829.

[107] Jespersen, N. D. *J. Am. Chem. Soc.* **1975**, *97*, 1662–1667.

[108] Clark, K. G.; Hetherington, H. C. *J. Am. Chem. Soc.* **1927**, *49*, 1909–1915.

[109] Clark, K. G.; Gaddy, V. L.; Rist, C. E. *Ind. Eng. Chem.* **1933**, *25*, 1092–1096.

[110] Wen, N.; Brooker, M. H. *J. Phys. Chem.* **1995**, *99*, 359–368.

[111] Amell, A. R. *J. Am. Chem. Soc.* **1956**, *78*, 6234–6238.

[112] Werner, R. C. *Journal of Biological Chemistry* **1942**, *142*, 705–723.

[113] Lynn, K. R. *J. Phys. Chem.* **1965**, *69*, 687–689.

[114] Shaw, W. H. R.; Walker, D. G. *J. Am. Chem. Soc.* **1957**, *79*, 4329–4331.

[115] Osetrova, N.; Skundin, A. *Elektrokhimiya* **2002**, *38*, 304–308.

[116] Rosendahl, S. M. Electrochemical and infrared spectroscopy studies of an ionizable self-assembled monolayer. Ph.D. thesis, University of Saskatchewan, 2009.

[117] Kamata, T.; Kato, A.; Umemura, J.; Takenaka, T. *Langmuir* **1987**, *3*, 1150–1154.

[118] Dovbeshko, G. I.; Chegel, V. I.; Gridina, N. Y.; Repnytska, O. P.; Shirshov, Y. M.; Tryndiak, V. P.; Todor, I. M.; Solyanik, G. I. *Biopolymers* **2002**, *67*, 470–486.

[119] Hartstein, A.; Kirtley, J. R.; Tsang, J. C. *Phys. Rev. Lett.* **1980**, *45*, 201–204.

[120] Nishikawa, Y.; Nagasawa, T.; Fujiwara, K.; Osawa, M. *Vibrational Spectroscopy* **1993**, *6*, 43–53.

[121] Bjerke, A. E.; Griffiths, P. R.; Theiss, W. *Anal. Chem.* **1999**, *71*, 1967–1974.

[122] Wan, L.-J.; Terashima, M.; Noda, H.; Osawa, M. *J. Phys. Chem. B* **2000**, *104*, 3563–3569.

[123] Osawa, M.; Ikeda, M. *J. Phys. Chem.* **1991**, *95*, 9914–9919.

[124] Hatta, A.; Ohshima, T.; Suëtaka, W. *Appl. Phys. A* **1982**, *29*, 71–75.

[125] Hatta, A.; Suzuki, Y.; Suëtaka, W. *Appl. Phys. A* **1984**, *35*, 135–140.

[126] Johnson, E.; Aroca, R. *J. Phys. Chem.* **1995**, *99*, 9325–9330.

[127] Merklin, G. T.; Griffiths, P. R. *Langmuir* **1997**, *13*, 6159–6163.

[128] Osawa, M.; Kuramitsu, M.; Hatta, A.; Suëtaka, W.; Seki, H. *Surface Science Letters* **1986**, *175*, L787–L793.

[129] Suzuki, Y.; Osawa, M.; Hatta, A.; Suëtaka, W. *Applied Surface Science* **1988**, *33*, 875–881.

[130] Wadayama, T.; Sakurai, T.; Ichikawa, S.; Suëtaka, W. *Surface Science* **1988**, *198*, L359–L364.

[131] Kuhne, C.; Steiner, G.; Fischer, W. B.; Salzer, R. *Fresenius J Anal Chem* **1998**, *360*, 750–754.

[132] Metiu, H. *Progress in Surface Science* **1984**, *17*, 153–320.

[133] Moskovits, M. *Rev. Mod. Phys.* **1985**, *57*, 783–826.

[134] Gersten, J. I.; Nitzan, A. *Surface Science* **1985**, *158*, 165–189.

[135] Bruggemann, D. *Ann. Phys.* **1935**, *24*, 665–679.

[136] Osawa, M. *Bulletin of the Chemical Society of Japan* **1997**, *70*, 2861–2880.

[137] Osawa, M.; Yoshii, K. *Applied Spectroscopy* **1997**, *51*, 512–518.

[138] Nakao, Y.; Yamada, H. *Surface Science* **1986**, *176*, 578–592.

[139] Nakao, Y.; Yamada, H. *Journal of Electron Spectroscopy and Related Phenomena* **1987**, *45*, 189–196.

[140] Krauth, O.; Fahsold, G.; Pucci, A. *Journal of Chemical Physics* **1999**, *110*, 3113.

[141] Aroca, R.; Price, B. *J. Phys. Chem. B* **1997**, *101*, 6537–6540.

[142] Yoshidome, T.; Inoue, T.; Kamata, S. *Chemistry Letters* **1997**, *26*, 533–534.

[143] Lu, G.-Q.; Sun, S.-G.; Chen, S.-P.; Cai, L.-R. *Journal of Electroanalytical Chemistry* **1997**, *421*, 19–23.

[144] Sato, S.; Kamada, K.; Osawa, M. *Chemistry Letters* **1999**, *28*, 15–16.

[145] Zhu, Y.; Uchida, H.; Watanabe, M. *Langmuir* **1999**, *15*, 8757–8764.

[146] Ortiz, R.; Cuesta, A.; Márquez, O. P.; Márquez, J.; Méndez, J. A.; Gutiérrez, C. *Journal of Electroanalytical Chemistry* **1999**, *465*, 234–238.

[147] Lu, G.-Q.; Sun, S.-G.; Cai, L.-R.; Chen, S.-P.; Tian, Z.-W.; Shiu, K.-K. *Langmuir* **2000**, *16*, 778–786.

[148] Watanabe, M.; Zhu, Y.; Uchida, H. *J. Phys. Chem. B* **2000**, *104*, 1762–1768.

[149] Huo, S.-J.; Xue, X.-K.; Yan,; Li, Q.-X.; Ma, M.; Cai, W.-B.; Xu, Q.-J.; Osawa, M. *J. Phys. Chem. B* **2006**, *110*, 4162–4169.

[150] Li, Q.-X.; Xue, X.-K.; Xu, Q.-J.; Cai, W.-B. *Appl Spectrosc* **2007**, *61*, 1328–1333.

[151] Osawa, M.; Ataka, K.-I.; Yoshii, K.; Nishikawa, Y. *Applied Spectroscopy* **1993**, *47*, 1497–1502.

[152] Hoffmann, F. M. *Surface Science Reports* **1983**, *3*, 107–192.

[153] Persson, B. N. J.; Ryberg, R. *Phys. Rev. B* **1981**, *24*, 6954–6970.

[154] Devlin, J. P.; Consani, K. *Journal of Physical Chemistry* **1981**, *85*, 2597–2598.

[155] Miyake, H.; Ye, S.; Osawa, M. *Electrochemistry Communications* **2002**, *4*, 973–977.

[156] Max, J.-J.; Chapados, C. *Appl Spectrosc* **2015**, *69*, 1281–1292.

[157] Penland, R. B.; Mizushima, S.; Curran, C.; Quagliano, J. V. *J. Am. Chem. Soc.* **1957**, *79*, 1575–1578.

[158] Srivastava, P. C.; Aravindakshan, C. *Zeitschrift fuer Physikalische Chemie (Leipzig)* **1983**, *264*, 61–64.

[159] Markovits, A.; García-Hernández, M.; Ricart, J. M.; Illas, F. *J. Phys. Chem. B* **1999**, *103*, 509–518.

[160] Greenler, R. G. *The Journal of Chemical Physics* **1966**, *44*, 310–315.

[161] Lebioda, L. *Acta Cryst. B* **1980**, *36*, 271–275.

[162] Redemann, C. E.; Riesenfeld, F. C.; Viola, F. S. L. *Ind. Eng. Chem.* **1958**, *50*, 633–636.

[163] Freund, H. J.; Roberts, M. W. *Surface Science Reports* **1996**, *25*, 225–273.

[164] Frasco, D. L. *The Journal of Chemical Physics* **1964**, *41*, 2134–2140.

[165] Yépez, O.; Scharifker, B. R. *Electrochimica Acta* **2005**, *50*, 1423–1429.

[166] Paul, D. K.; McKee, M. L.; Worley, S. D.; Hoffman, N. W.; Ash, D. H.; Gautney, J. *J. Phys. Chem.* **1989**, *93*, 4598–4603.

[167] Corrigan, D. S.; Weaver, M. J. *J. Phys. Chem.* **1986**, *90*, 5300–5306.

[168] Bron, M.; Holze, R. *Journal of Electroanalytical Chemistry* **1995**, *385*, 105–113.

[169] Brandt, K.; Vogler, E.; Parthenopoulos, M.; Wandelt, K. *Journal of Electroanalytical Chemistry* **2004**, *570*, 47–53.

[170] Bron, M.; Holze, R. *Fresenius J Anal Chem* **1998**, *361*, 694–696.

[171] Corrigan, D. S.; Weaver, M. J. *Langmuir* **1988**, *4*, 599–606.

[172] Rosendahl, S. M.; Danger, B. R.; Vivek, J. P.; Burgess, I. J. *Langmuir* **2009**, *25*, 2241–2247.

[173] Lachenwitzer, A.; Magnussen, O. M. *J. Phys. Chem. B* **2000**, *104*, 7424–7430.

[174] Pensa, E.; Vericat, C.; Grumelli, D.; Salvarezza, R. C.; Park, S. H.; Longo, G. S.; Szleifer, I.; Leo, L. P. M. D. *Phys. Chem. Chem. Phys.* **2012**, *14*, 12355–12367.